

Article

# Genetic and Epigenetic Regulation of Zebrafish Intestinal Development

Bilge San <sup>1</sup>, Marco Aben <sup>1,2</sup>, Dei M. Elurbe <sup>1,2</sup>, Kai Voeltzke <sup>2,†</sup>, Marjo J. den Broeder <sup>3,‡</sup>, Julien Rougeot <sup>2</sup>, Juliette Legler <sup>3,‡</sup> and Leonie M. Kamminga <sup>1,2,\*</sup>

<sup>1</sup> Department Molecular Biology, Radboud Institute for Molecular Life Sciences, Radboud University Medical Centre, 6525 GA Nijmegen, The Netherlands; sanbilge@gmail.com (B.S.); marco.aben@radboudumc.nl (M.A.); d.elurbe@science.ru.nl (D.M.E.)

<sup>2</sup> Department Molecular Biology, Radboud Institute for Molecular Life Sciences, Faculty of Science, Radboud University, 6525 GA Nijmegen, The Netherlands; kai\_uni@rocketmail.com (K.V.); j.rougeot@science.ru.nl (J.R.)

<sup>3</sup> Institute for Environmental Studies, Vrije Universiteit Amsterdam, 1081 HV Amsterdam, The Netherlands; m.j.denbroeder@uu.nl (M.J.d.B.); j.legler@uu.nl (J.L.)

\* Correspondence: l.kamminga@science.ru.nl; Tel.: +31-24-361-6850

† Current address: Department of Pediatric Oncology, Hematology, and Clinical Immunology, University Hospital Düsseldorf, 40225 Düsseldorf, Germany.

‡ Current address: Institute for Risk Assessment Sciences, Utrecht University, 3584 CM Utrecht, The Netherlands.

Received: 23 August 2018; Accepted: 18 October 2018; Published: 23 October 2018



**Abstract:** Many regulatory pathways are conserved in the zebrafish intestine compared to mammals, rendering it a strong model to study intestinal development. However, the (epi)genetic regulation of zebrafish intestinal development remains largely uncharacterized. We performed RNA-sequencing and chromatin immunoprecipitation (ChIP)-sequencing for activating (H3K4me3) and repressive (H3K27me3) chromatin marks on isolated intestines at 5, 7, and 9 days post-fertilization (dpf), during which zebrafish transit from yolk dependence to external feeding. RNA-sequencing showed the enrichment of metabolic maintenance genes at all time points and a significant increase in lipid metabolism between 5 and 9 dpf. A strong correlation was observed between gene expression and presence of chromatin marks on gene promoters; H3K4me3-marked genes were expressed higher than H3K27me3-marked genes. Next, we studied a key epigenetic player, Enhancer of zeste homolog 2 (Ezh2). Ezh2 places the repressive H3K27me3 mark on the genome and is highly conserved in vertebrates. We used the nonsense mutant allele *ezh2(hu5670)* to study the effect of *ezh2* loss on intestinal development. These mutants survived gastrulation and died around 11 dpf, showing severe morphological defects in the intestine and liver, accompanied by decreased intestinal (*fabp2*) and hepatic (*fabp10a*) marker expressions. Our results suggest that Ezh2 is essential for proper intestinal tissue maintenance and overall survival.

**Keywords:** zebrafish; development; ENU mutagenesis; Polycomb repressive complex 2; gene expression; transcriptomics; epigenetics; Ezh2

## 1. Introduction

Multicellular organisms develop from a single cell to a complex architecture of tissues, which requires tightly regulated stepwise processes such as cell specification, tissue expansion, and maintenance of organ function. For each of these processes, a series of cellular decisions are made to regulate which genes in the genome are to be cell- or tissue-specifically transcribed or repressed. The eventual transcriptome of the cell designates its identity and function [1,2].

Several covalent epigenetic modifications have been found to directly affect the transcriptome that ranges from DNA methylation to an array of post-translational histone modifications. The rate of compaction and flexibility of nucleosomes affect the accessibility of genes around specific histone modifications [3]. All modifications combined allow for a cell-specific balance between active and repressed genes. Two well-characterized modifications are histone H3 lysine 4 trimethylation (H3K4me3) and histone H3 lysine 27 trimethylation (H3K27me3), which are prominent indicators of active and repressed genes, respectively. H3K4me3 is deposited by Trithorax complexes [4] on gene promoters and is thought to be instructive for transcription [5]. H3K27me3, on the other hand, is deposited by Polycomb complexes and can localize on promoters and gene bodies [4]. The presence of Polycomb complexes on the genome strongly correlates with a repressed chromatin state [6]. Reports in recent years indicate that the loss of H3K4me3 does not affect transcription to a large degree [7] and that not all H3K27me3-marked genes become repressed [8]. Moreover, genes marked by both H3K4me3 and H3K27me3 can be repressed, poised for activation, or active [9,10]. Gene repression is a complex process, and more research is crucial to gain insight on the interplay between epigenetic marks and their impact on cellular regulation.

Polycomb group proteins are well-conserved transcriptional gene silencers and function mainly in two protein complexes: Polycomb Repressive Complex 1 and 2 (PRC1 and PRC2) [11]. PRC2 is highly conserved in vertebrates [12] and has three core components; EZH1/2 (Enhancer of Zeste Homolog 1/2), SUZ12 (Suppressor of Zeste 12 homolog), and EED (Embryonic Ectoderm Development) [13,14]. PRC1 components, on the other hand, are highly variable in vertebrates [15,16]. The PRC1-complex always includes RING1A/B (Ring Finger Protein 1A/B) and frequently the CBX (Chromobox), RYBP (RING1 And YY1 Binding Protein), PHC (Polyhomeotic-like Protein), and BMI (B Lymphoma Mo-MLV Insertion Region 1) variants, and its function differs according to its composition [16–18]. The classical view is that gene repression by the PRC1/2 complexes occurs in two steps: first, EZH1/2 trimethylates lysine 27 of histone H3 (H3K27me3) on a specific gene locus. Subsequently, PRC1 is recruited to the H3K27me3 mark and its catalytic component RING1A/B mono-ubiquitylates lysine 119 of histone H2A (H2AK119Ub) [19,20]. Together, these two events lead to the compaction of histones at the locus and result in gene repression. Although the classical view indicates that the placement of H3K27me3 and H2AK119Ub on a gene is causative for gene repression, it has been suggested that nucleosome compaction, gene silencing, and PRC1 itself can trigger PRC1 and PRC2 action [21,22].

Both the up- and down-regulation of EZH2—the catalytic subunit of PRC2—has been associated with several types of cancers in humans [23]; the protein is considered as a promising target for the development of cancer inhibitory drugs [24]. In general, loss of function mutations and overexpression of the PRC2 complex have drastic effects on tissue-specification and maintenance in many organisms [25]. Mutations in the *ezh2* homolog *E(z)* in the fruit fly cause the anteriorization of *Hox* gene expression [26]. *Ezh2* mutations in mice lead to early embryonic lethality [27,28], and therefore, most murine studies have focused on tissue-specific knockout models [29–31]. Accumulating evidence assigns tissue-specific functions to *Ezh2*, such as control over progenitor pools [32–36], terminal cell differentiation [37], or maintenance [36,38–40]. Therefore, the further characterization of its function in an intact, whole animal, such as the zebrafish, is needed to further our understanding of the function of this protein.

Zebrafish is one of the most favorable vertebrate model organisms to study mutations and diseases. In addition to low cost and relative ease of husbandry, their high fecundity provides researchers with an easy access to large clutches of synchronously developing embryos. Importantly, there is a high conservation of fundamental (vertebrate) gene regulation pathways [41]. The developmental gene regulatory systems of the zebrafish intestine are conserved in higher vertebrates, despite some differences during the development of the organ primordium [42,43]. The zebrafish intestine is derived from a primitive gut tube, from which the liver and pancreas bud off and develop independently [44,45]. Subsequently, the intestine develops into three main regions: the intestinal bulb (IB), mid-intestine (MI), and posterior intestine (PI). One should keep in mind that the zebrafish

is a stomachless species. The intestinal epithelium is folded irregularly into ridges to enlarge the absorptive surface, an organization somewhat reminiscent of the villous epithelium of mammals [43]. By 5 days post-fertilization (dpf), the yolk is largely absorbed and the zebrafish larvae start feeding exogenously, while the intestine continues maturing throughout the second week of development [46]. The epithelium is rich in enterocytes (in IB, MI) and goblet cells (in MI), and enteroendocrine cells are scattered throughout the intestine [46]. The zebrafish intestinal epithelium is simpler than that of mammals as it lacks crypts of Lieberkühn and the thin muscularis mucosa. The epithelium and mucosal layers are enclosed by circular and longitudinal smooth muscle layers and a serosa [43]; in between the latter myenteric neurons are positioned, which control intestinal motility [47].

In mammals, PRC2 has been implicated as an important regulator of intestinal epithelial proliferation [48]. The expression of its components decreases as cells differentiate. Depletion of EZH2 diminishes colorectal cancer proliferation in humans [49]. Many transcription factors (e.g., CDX, GATA) [50,51] and cell signaling pathways (e.g., Delta-Notch [52]) have been found in the intestines of zebrafish and higher vertebrates alike [53]. The transition of zebrafish embryos from lecithotrophy, i.e., yolk dependency, to a free-feeding larva is a very rapid process, which predictably requires extensive transcriptional and epigenetic regulation. To delineate these regulatory processes, we focused on the (epi)genetic regulation of transcription in the zebrafish intestine, particularly by PRC2. We hypothesized that the loss of *Ezh2* would likely cause intestinal defects by transcriptional changes resulting from aberrant gene repression.

We present an in-depth analysis of the wild-type transcriptome, as well as the presence of H3K4me3 and H3K27me3 on gene promoters in the larval zebrafish intestine at 5, 7, and 9 days post-fertilization (dpf). This was made possible by our novel approach of rapid and efficient intestinal dissection using the intestine-specific transgene *tgBAC(cldn15la:GFP)*. We demonstrate that zygotic *ezh2* mutants (*ezh2*<sup>-/-</sup>) gastrulate normally and undergo organogenesis similarly as wild-type siblings until 5 dpf, but die around 11 dpf, displaying loss of intestinal and hepatic tissue maintenance. Our results suggest that *Ezh2* is essential for the proper development and function of the intestinal tract and the survival of zebrafish larvae.

## 2. Results

### 2.1. The Intestinal Transcriptome in Wild-Type Zebrafish Larvae

To study the larval wild-type intestinal transcriptome, we dissected intestines from 5, 7, and 9 dpf zebrafish in the *tgBAC(cldn15la:GFP)* background (Figure 1A). This intestinal transgene expresses the GFP-tagged intestine-specific tight junction protein Claudin 15-like a [54]. After dissection, we performed whole transcriptome RNA sequencing. We analyzed the genes that were constitutively expressed in the intestine across 5, 7, and 9 dpf, as well as genes that were differentially expressed between the three time points in groups of two; 5 vs 7 dpf, 7 vs 9 dpf, and 5 vs 9 dpf. GO and anatomical term analyses were performed for gene categories extracted from the dataset.

Principal component analysis using the top 500 differentially expressed genes at all time points and replicates showed that 53% of the variation between samples could be explained by developmental time point differences as well as distinction between replicates (Figure 1B); 5 and 9 dpf intestinal replicates fell into distinct clusters, and 7 dpf replicates appeared more related to 9 dpf than 5 dpf. This result was also reflected in the Euclidean distance between samples using all genes; 5 and 9 dpf expression patterns were distinct from each other and 7 dpf replicates appeared more related to 9 dpf than 5 dpf (Figure 1C).

Fragments Per Kilobase of transcript per Million (FPKM)  $\geq 1$  in 2 out of 3 replicates was set as a threshold for gene expression for each time point. According to this threshold, 21,507 out of 32,266 annotated zebrafish genes (66.7%) were constitutively expressed in dissected intestines at 5, 7, and 9 dpf, and 10,759 genes (33.3%) were not expressed (FPKM  $< 1$  in 2 out of 3 replicates at 5, 7, and 9 dpf). Out of 1001 larval (3–30 dpf) genes which were anatomically characterized to have intestinal

expression on the Zebrafish Information Network (ZFIN) [55], 855 genes showed expression at all time points in our dataset, indicating the significant enrichment of intestinal genes in this dataset ( $p < 0.001$ ,  $\chi^2$  significance test). Among these genes were enterocyte (*vps51*), goblet (*agr2*), enteroendocrine (*gcca*), and putative stem cell (*lgr4*) specific markers, intestinal transcription factors (*cdx1b*, *gata4/5/6*, *foxa3*, *acsl1b*, *klf4*), genes involved in peptide (*pepd*), lipid (*lipf*, *apoa4a*), water (*aqp3a*), and glucose (*slc5a1*) metabolism, and cell signaling pathway components (*apc*, *notch2*, *fgfr4*, *shha*, *bmp2b*, *egfra*, *tgfb1a*) (Figure 1D). The consistent expression of these genes suggests that the dataset is specific to the intestine and allows the extraction of intestinal cell type-specific gene expression. Indeed, the comparison of transcriptomic data generated from 5 dpf whole larvae (publicly available [56]) and 5 dpf intestines demonstrated that the brain-, cardiovascular-, epidermis-, eye-, liver-, and pancreas-specific genes are expressed significantly less in the intestinal transcriptome, whereas intestine-specific genes are significantly enriched in the intestinal transcriptome (Figure S1). Additionally, PRC2 complex components were expressed at all time points (Figure 1D). The zebrafish homolog of the Trithorax group protein MLL1, *kmt2a*, which putatively places the H3K4me3 mark on the genome, was also expressed at all time points (Figure 1D). The top 5000 genes expressed at all three time points were enriched for translation, the peptide biosynthetic process, and the peptide metabolic process (Figure 1E, Table S1.1). These top 5000 genes were also highly enriched for the liver, intestinal bulb, and gut in anatomical terms (Figure 1F; Tables S1.2 and S1.3).

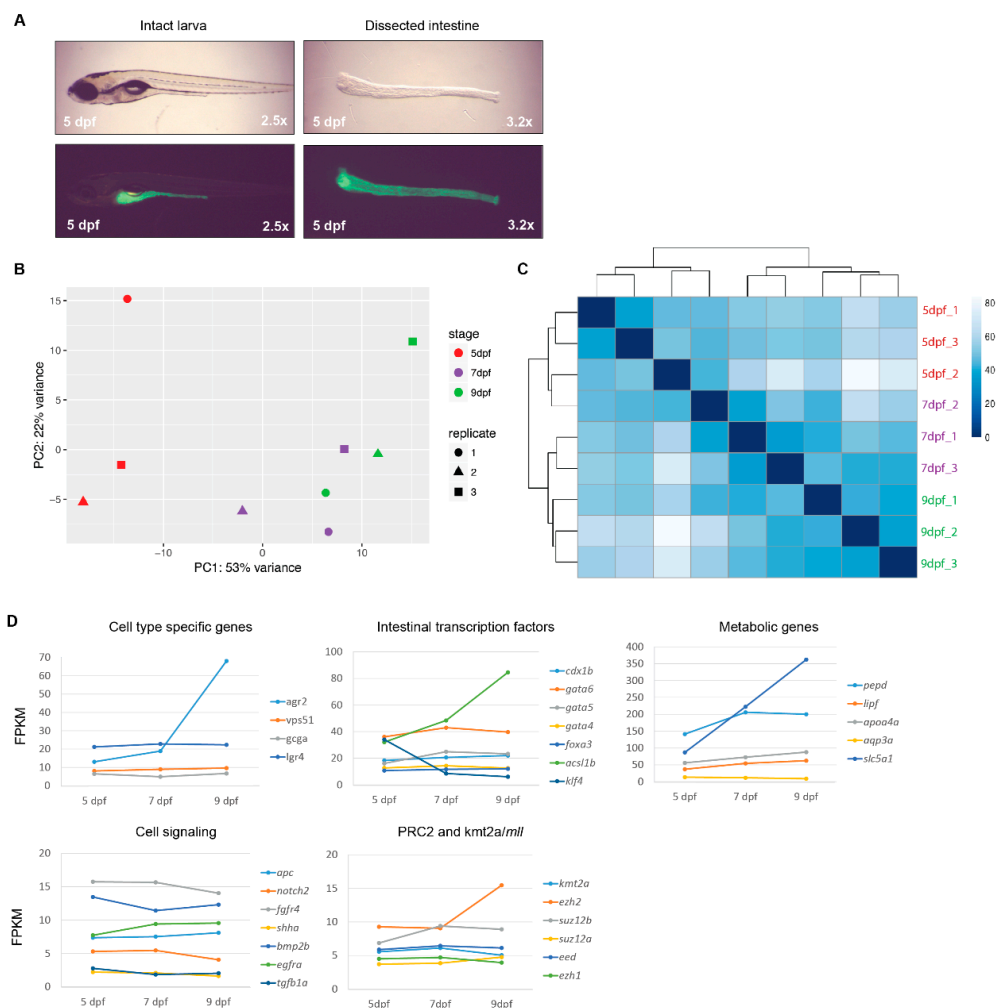
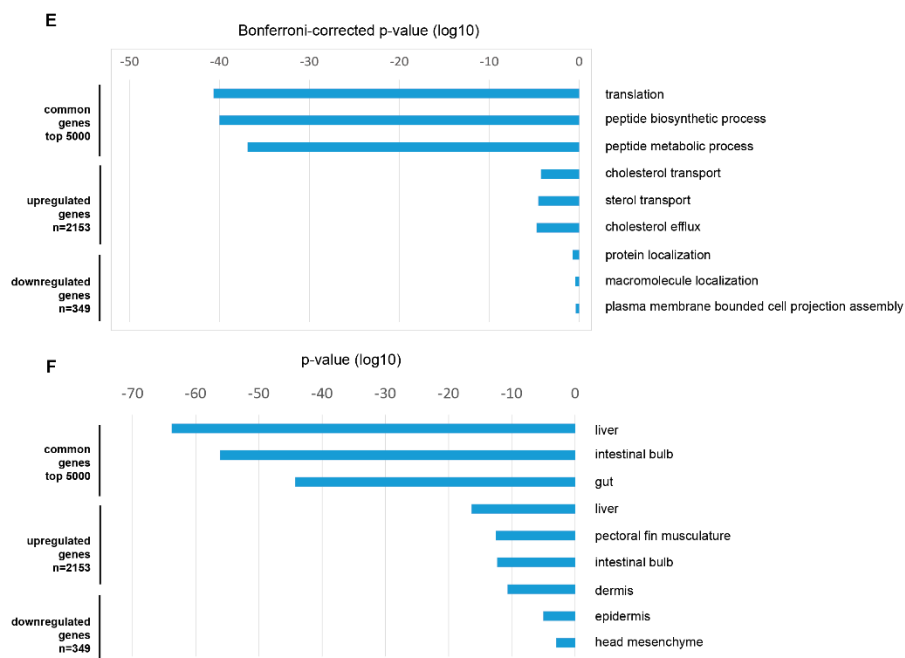


Figure 1. Cont.



**Figure 1.** The RNA-sequencing on wild-type larval zebrafish intestines. **(A)** Intestines were dissected from 5, 7, and 9 dpf larvae in the *tgBAC (cldn15la:GFP)* background. A 5 dpf larva is shown as an example. The intestine is pulled out of the intact body (left panels) with the use of tweezers, and subsequently cleaned up of non-intestinal tissues. The resulting pure intestines (right panel) are pooled in tubes and used for RNA- or ChIP-sequencing. The bottom right of each panel indicates magnification on a 10 $\times$  objective. Top: light, bottom: fluorescence microscopy. **(B)** Two-dimensional principal component analysis on the top 500 differentially expressed genes in the RNA-sequencing dataset indicates that based on these genes 53% of the variation can be explained by a developmental time point and replicate differences. Red dots: 5 dpf; purple dots: 7 dpf, green dots: 9 dpf. Replicates are indicated by different shapes (circle, triangle, square). **(C)** Heat map displaying the Euclidean distances between all samples in all genes shows distinct clustering of 5 and 9 dpf replicates. One out of three 7 dpf replicates is more similar to 5 dpf, and two out of three are more similar to 9 dpf. Replicate numbers and colors match the replicates depicted in A. **(D)** Normalized average gene expression levels (FPKM) of a selection of genes in the larval wild-type intestines at 5, 7, and 9 dpf. Intestinal cell type-specific genes, intestinal transcription factors, metabolic genes, cell signaling components, PRC2 subunits, and the Trithorax *kmt2a* are expressed at 5, 7, and 9 dpf. **(E)** Top three gene ontology terms (GOrrilla) enriched for 5000 genes expressing the highest at all time points, and significantly upregulated and downregulated genes between 5 and 9 dpf, depicted by log10 of Bonferroni corrected p-values. **(F)** Top three anatomical terms (ZEOGS) enriched for 5000 genes expressing the highest at all time points, and significantly upregulated and downregulated genes between 5 and 9 dpf, depicted by log10 of *p*-values.

Next, differential gene expression between time points was analyzed. The significance threshold for differential gene expression was set at  $\text{padj} < 0.01$  and  $|\text{LFC}| > 0$ . From 5 to 7 dpf, 556 genes were significantly upregulated, and 224 genes were significantly downregulated. From 7 to 9 dpf, 278 genes were significantly upregulated, and 51 genes were significantly downregulated. As predicted, the highest gene expression differences were between 5 and 9 dpf, where 2153 genes were significantly upregulated and 349 genes were significantly downregulated. The GO terms enriched for genes upregulated from 5 to 9 dpf were of cholesterol transport, sterol transport, and cholesterol efflux. Downregulated genes were non-significantly ( $p > 0.1$ ) enriched for protein/macromolecule localization and plasma membrane-bounded cell projection assembly (Figure 1E; Tables S2.1 and S3.1). The top three anatomical terms enriched for upregulated genes were liver, pectoral fin musculature, and

intestinal bulb. The downregulated genes showed enrichment for dermis, epidermis, and head mesenchyme (Figure 1F, Tables S2.2, S2.3, S3.2, and S3.3). These results suggest that between 5 and 9 dpf, the larval zebrafish intestine continues maturing and the expression of genes important for the metabolism dynamically increases over time, whereas there is a decrease in extra-intestinal gene expression.

To continue the molecular characterization of the larval zebrafish intestine, we performed ChIP-sequencing for the histone marks H3K4me3 and H3K27me3 on dissected intestines at 5, 7, and 9 dpf.

## 2.2. H3K4me3-Marked Promoters and Gene Expression in the Larval Intestine

In dissected zebrafish intestines, H3K4me3 was found on 12,504, 13,330, and 13,955 gene promoters at 5, 7, and 9 dpf, respectively. We analyzed gene promoters commonly and distinctly marked by H3K4me3 at each time point and compared the gene expression status (FPKM  $\geq 1$ ) for each category. Most genes ( $N = 12,329$ ) were commonly marked by H3K4me3 at all time points (Figure 2A). The analysis showed that an average of 95% of H3K4me3-marked genes were expressed in the intestine at each time point, as well as genes commonly marked at all time-points (11,657 expressed out of 12,329 commonly marked genes). Next to genes that were marked by H3K4me3 at all time points, we also detected genes that gained or lost the H3K4me3 mark between time points. However, the loss or gain of H3K4me3 between time points did not correlate with changes in gene expression; i.e., genes that gained the activating H3K4me3 mark over time did not consistently increase in expression, and genes that lost H3K4me3 over time did not consistently get decreased in expression (Figure S2A). A comparison of differential gene expression between 5–7, 7–9, and 5–9 dpf and the presence of H3K4me3 on gene promoters at the compared time points can be found in Tables S4, S5, and S6, respectively.

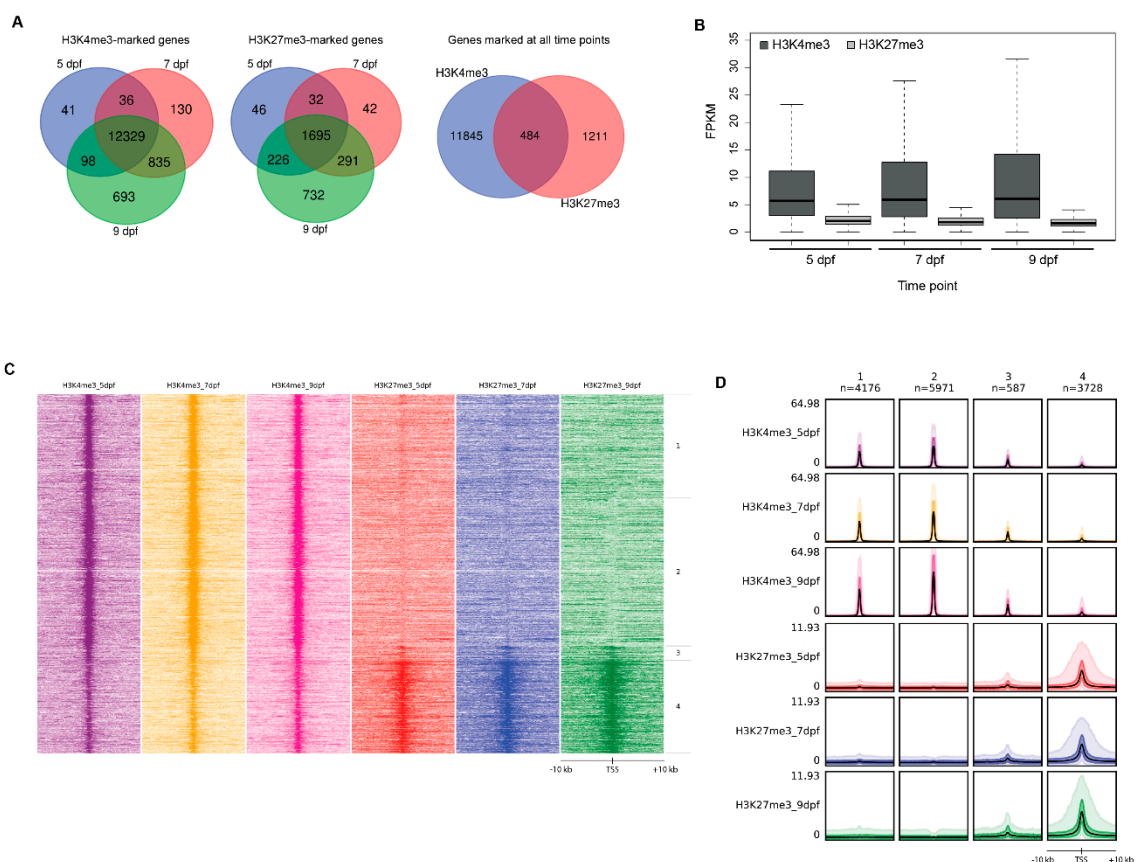
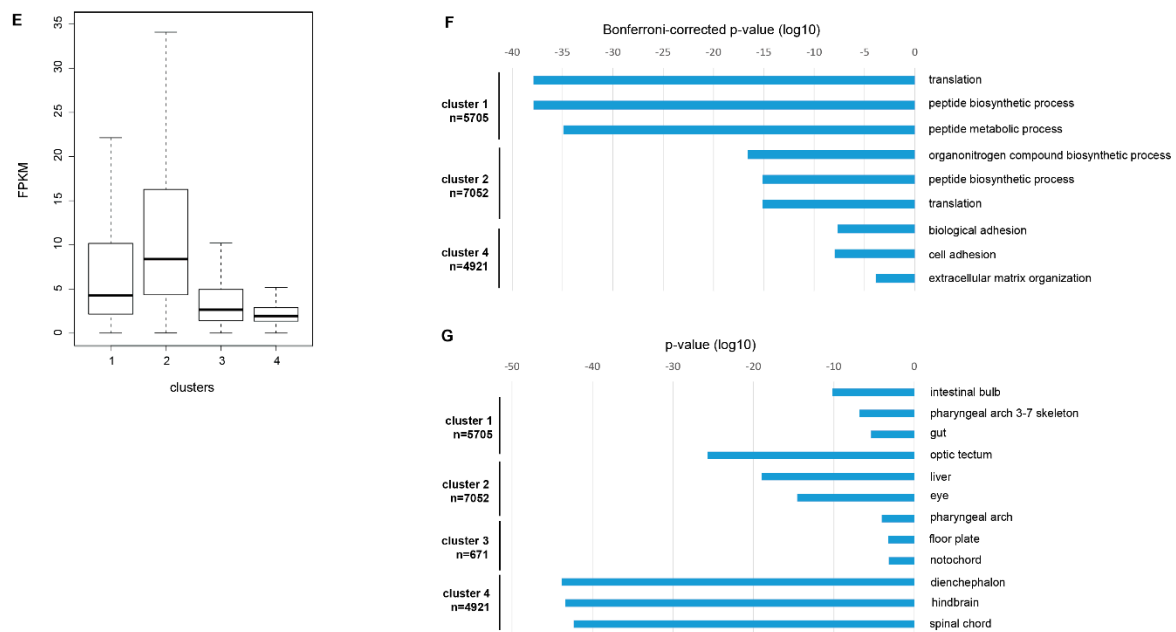


Figure 2. Cont.



**Figure 2.** The ChIP-sequencing for H3K4me3 and H3K27me3 on wild-type larval zebrafish intestines. (A) Venn diagrams indicating the number of common genes marked by H3K4me3 (left) and H3K27me3 (middle) on promoter regions at 5, 7, and 9 dpf, and the overlap of genes marked at all time points by H3K4me3 and H3K27me3 (right). Circle sizes are not relative. (B) Box plot showing the FPKM expression values of genes commonly marked at 5, 7, and 9 dpf with H3K4me3 (dark grey) and H3K27me3 (light grey) on promoter regions. H3K27me3 marked genes show a lower expression compared to H3K4me3. (C) Heat map and (D) band plot of 4 clusters formed by all H3K4me3 and H3K27me3 peaks on gene promoters across developmental time points. The number of peaks per cluster is indicated above. Cluster 1 and 2 show high H3K4me3 and near absent H3K27me3 levels, cluster 3 shows low H3K4me3 and H3K27me3 levels, and cluster 4 shows the lowest H3K4me3 and highest H3K27me3 levels of all clusters. Genomic window:  $\pm 10$  kb. In the band plot, the mean of the median is depicted as a black line, the intense color in 50% of the peaks, and the light color in 90% of the peaks. (E) Box plots of FPKM expression values of expressed genes from clusters in C, D. Clusters 1 and 2, which are marked by high H3K4me3 and low H3K27me3 peaks, show higher gene expression levels than genes from clusters 3 and 4, which are marked by low H3K4me3 and high H3K27me3 peaks. (F) Top three gene ontology terms (GO) enriched for genes marked in each cluster in C, D, depicted by the  $\log_{10}$  of Bonferroni corrected  $p$ -values. (G) Top three anatomical terms (ZEOGS) enriched for genes marked in each cluster in C, D, depicted by the  $\log_{10}$  of  $p$ -values.

GO-term and anatomical term analyses for H3K4me3-marked genes showed a high overlap with that of the transcriptome. For H3K4me3-marked genes, the enriched molecular processes were the translation, the peptide biosynthetic process, and the peptide metabolic process (Figure S3A, Table S7.1). The top enriched anatomical terms were the liver, gut, and intestinal bulb (Figure S3B; Tables S7.2 and S7.3). These results indicate that H3K4me3-marked genes in the larval zebrafish intestine are indeed intestine-specific and are expressed.

### 2.3. H3K27me3-Marked Promoters and Gene Expression in the Larval Intestine

The repressive H3K27me3 mark is initially placed in gene promoters, after which it spreads to the gene bodies [57]. For better comparison with the H3K4me3 mark, we analyzed the presence of H3K27me3 in promoters in dissected zebrafish intestines. The H3K27me3 mark was found on 1999, 2060, and 2944 gene promoters at 5, 7, and 9 dpf, respectively, out of which 1695 genes were commonly marked at all time points (Figure 2A). Surprisingly, for this repressive mark, an average of 85% of genes marked on promoters were expressed at each time point (FPKM  $\geq 1$  in 2 out of 3 replicates).

Gain or loss of H3K27me3 on gene promoters over time did not correlate with the gene expression changes; genes that gained H3K27me3 over time did not get repressed, and genes that lost H3K27me3 over time did not show an upregulation (Figure S2B). A comparison of differential gene expression between 5–7, 7–9, and 5–9 dpf and the presence of H3K27me3 on gene promoters at the compared time points can be found in Tables S4, S5, and S6, respectively.

Next to promoters, we have analyzed the presence of H3K27me3 in gene bodies (Figure S4A) and intergenic regions (Figure S4B), and detected no prominent changes between 5, 7, and 9 dpf.

GO-term enrichment for genes marked by H3K27me3 on promoters was highest for anatomical structure development, multicellular organismal processes, and developmental processes (Figure S3A, Table S8.1), whereas the top anatomical terms for H3K27me3-marked genes were neuronal structures such as the diencephalon, hindbrain, and spinal cord (Figure S3B; Tables S8.2 and S8.3). GO and anatomical term analyses indicate that in the larval zebrafish intestine, H3K27me3 covers gene promoters of genes controlling embryonic development and extra-intestinal lineage genes.

#### 2.4. Comparison of H3K4me3- and H3K27me3-Marked Promoters

Out of all genes marked by H3K4me3 ( $n = 12,329$ ) and H3K27me3 ( $n = 1695$ ) on promoters at all time points, 484 gene promoters showed an overlap of both histone marks, whereas most genes were distinctly marked by H3K4me3 ( $n = 11,845$ ) or H3K27me3 ( $n = 1211$ ), as depicted in Figure 2A. Interestingly, these 484 genes were enriched for transcriptional/RNA regulation (Figure S3A, Table S9.1), and for neuronal anatomical structures (Figure S3B; Tables S9.2 and S9.3). Despite the high percentage of gene expression observed for genes marked by H3K4me3 (95% expressed) and H3K27me3 (85% expressed), H3K27me3-marked genes were expressed at a much lower level than H3K4me3-marked genes (Figure 2B).

H3K4me3- and H3K27me3-marked transcription start sites clustered in 4 major groups, represented as a heat map (Figure 2C) and a band plot (Figure 2D) with a window length of  $\pm 10$  kilobases. Cluster 1 ( $N = 5705$ , 84% FPKM  $\geq 1$ ) and cluster 2 ( $N = 7052$ , 95% FPKM  $\geq 1$ ) were composed of high H3K4me3 and near absent H3K27me3 peaks. Cluster 3 ( $N = 671$ , 79% FPKM  $\geq 1$ ) presented low H3K4me3 and H3K27me3 peaks. Cluster 4 ( $N = 4921$ , 74% FPKM  $\geq 1$ ) showed the lowest H3K4me3 levels of all 4 clusters and the highest H3K27me3 peak intensity. Strikingly, as indicated above for each cluster (depicted in parentheses), high H3K4me3 and low H3K27me3 peaks were positively correlated with the percentage of expressed genes (FPKM  $\geq 1$ ). Additionally to gene expression status, high H3K4me3 and low H3K27me3 peaks were positively correlated with the level of gene expression as well (Figure 2E).

Following the trend for the positive correlation between the H3K4me3 presence and gene expression, GO term analysis showed that cluster 1 was highly enriched for translation and peptide biosynthetic/metabolic processes. Cluster 2 was enriched for the organonitrogen compound biosynthetic process, the peptide biosynthetic process, and translation. Cluster 3 did not yield a significant GO term enrichment. Cluster 4, which had the highest H3K27me3 presence, showed enrichment for biological adhesion, cell adhesion, and extracellular matrix organization (Figure 2F, Tables S10.1, S11.1, S12.1, and S13.1). Anatomical terms enriched for cluster 1 were the intestinal bulb, pharyngeal arch 3–7 skeleton, and gut. For cluster 2, the optic tectum, liver, and eye were enriched. Cluster 3 showed enrichment for genes expressed in the pharyngeal arch, floor plate, and notochord. Lastly, cluster 4 was enriched for the diencephalon, hindbrain, and the spinal cord (Figure 2G, Tables S10.2, S10.3, S11.2, S11.3, S12.2, S12.3, S13.2, and S13.3).

Overall, in our epigenetic analysis on zebrafish intestinal lysates at 5, 7, and 9 dpf, H3K4me3 was correlated with a high gene expression and intestinal metabolic genes, whereas H3K27me3 was correlated with a low expression and extra-intestinal genes. Examples of genome browser tracks of H3K4me3 and H3K27me3 in the intestine at 5, 7, and 9 dpf on the Wnt pathway component *apc*, intestinal transcription factors *cdx1b* and *gata5*, the pluripotency factor *klf4*, and the PRC2 target *hoxd* gene cluster can be found in Figure S5.

### 2.5. Expression of *ezh1* and *ezh2* in Whole Embryos and Larvae

PRC2 is crucial for correct tissue maintenance and survival, and its components Ezh1 and Ezh2 are both enzymatically able to set the H3K27me3 mark [29,58,59]. Moreover, Ezh2 is crucial for the correct development in zebrafish; its maternal and zygotic loss leads to lethality at 2 dpf [60]. The developmental function of Ezh1 in zebrafish is currently unknown. To assess the expression dynamics between *ezh1* and *ezh2* during development, their mRNA expression profiles were quantified by RT-qPCR in whole wild-type embryos and larvae from 4 cells until 15 dpf (Figure 3A). Supporting previous research [60,61], the *ezh1* mRNA was not detectable in embryos until 1 dpf, while its expression continuously increased until 6 dpf. After 6 dpf, the expression of *ezh1* gradually decreased, with yet another increase observed at 15 dpf. At the 4–16 cell stage, the *ezh2* mRNA was already present, confirming that it is maternally provided [60,61]. Its expression peaked at 4 hpf around zygotic gene activation, and it gradually decreased until the larval stages were reached. Between 5 and 15 dpf, this lower expression level was maintained with small fluctuations.

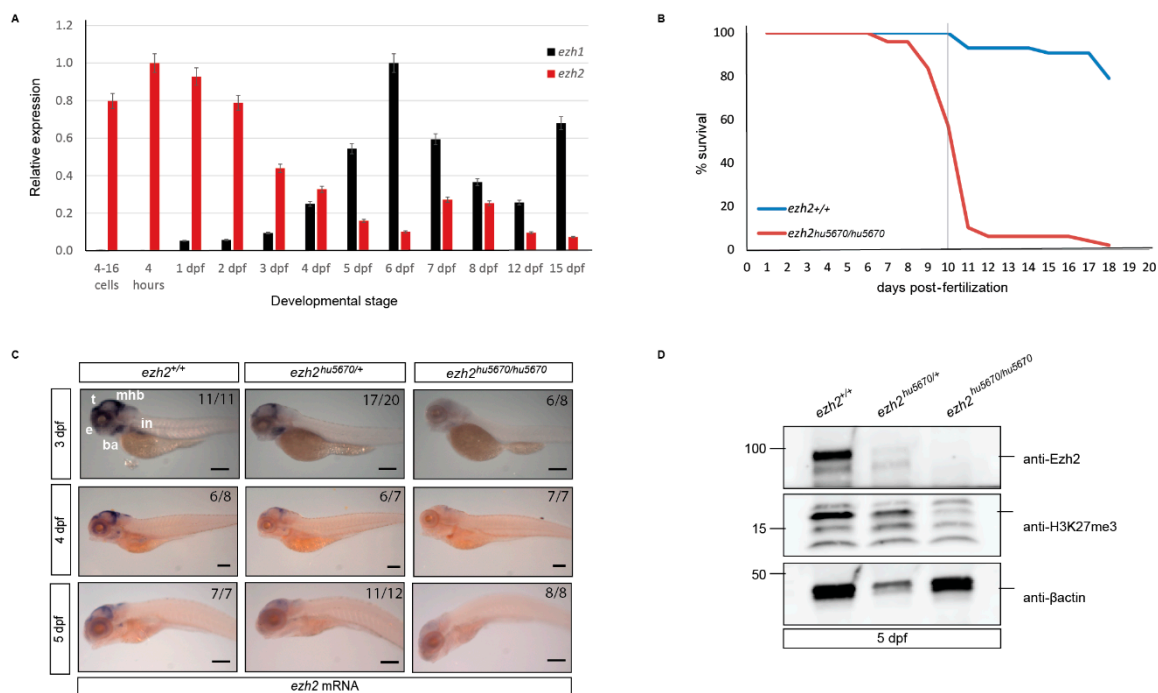


**Figure 3.** The characterization of zygotic *ezh2* mutants. **(A)** RT-qPCR analysis of *ezh1* and *ezh2* expression in wild-type zebrafish embryos and larvae in a developmental time series from 4 cells until 15 dpf. Four biological, three technical replicates were used. The expression of *ezh1* and *ezh2* were normalized to reference genes  $\beta$ -actin, *hprt1*, *rps18*, and *ef1a*. Error bars represent the standard error of the mean. **(B)** Survival of wild-type ( $N = 43$ ) and *ezh2*<sup>-/-</sup> ( $N = 49$ ) zebrafish. The *ezh2* mutants predominantly die between 10–11 dpf, while 79% of the wild-type larvae are alive at 19 dpf, the end of the experiment. Additionally, 10 dpf is marked by a semi-transparent vertical line. **(C)** Whole-mount in-situ hybridization of 3, 4, and 5 dpf embryos for *ezh2* expression. At 3 dpf, *ezh2* is expressed in the eye (e), tectum (t), mid-hindbrain boundary (mhb), branchial arches (ba), and intestine (in) in wild-type siblings. The wild-type expression is spatially more restricted at 4 and 5 dpf. In *ezh2*<sup>+/-</sup>, a smaller *ezh2* expression is observed compared to wild-types at all time points, while in *ezh2*<sup>-/-</sup> embryos, the *ezh2* expression is predominantly diminished. Numbers indicate observation of expression per total embryos analyzed. Scale bar: 200  $\mu$ m. **(D)** Western blot for Ezh2 (top, 85 kDa), H3K27me3 (middle, 15 kDa), and  $\beta$ -actin (bottom, 42 kDa) in the wild-type (left), *ezh2*<sup>+/-</sup> (middle), and *ezh2*<sup>-/-</sup> (right) sibling larvae at 5 dpf. In *ezh2*<sup>-/-</sup> larvae, Ezh2 protein expression is lost, H3K27me3 is decreased compared to wild-types and heterozygotes. Numbers on the left indicate protein marker positions, lines on the right indicate the position of the protein.

## 2.6. Characterization of the Zygotic *ezh2* (*hu6570*) Mutant Zebrafish

To analyze the role of transcriptional repression in the zebrafish larval intestine in greater detail, we used an *ezh2* allele (*hu5670*, R592STOP) with a nonsense mutation upstream of the SET methyltransferase domain, generated by ENU-induced random mutagenesis [62]. Our model retains maternal *ezh2* contribution in earlier embryonic stages but lacks zygotic *ezh2* expression. Henceforth, we refer to this zygotic mutant as *ezh2*<sup>-/-</sup>.

We assessed the survival of *ezh2*<sup>-/-</sup> zebrafish in comparison with wild-type siblings. The larvae mutants for *ezh2* ( $N = 49$ ) apparently go through gastrulation and organogenesis yet die around 11 dpf. Wild-type siblings ( $N = 43$ ) showed around an 80% survival (Figure 3B). We performed whole-mount in-situ hybridization (WISH) to compare *ezh2* mRNA expression between *ezh2*<sup>-/-</sup> mutants and their heterozygous and wild-type siblings at 3, 4, and 5 dpf (Figure 3C). In 3 dpf wild-type and heterozygous siblings, *ezh2* was expressed in the eye, tectum, otic vesicle, mid-hindbrain boundary, branchial arches, and the intestine. At 4 dpf, *ezh2* expression was detectable in the mid-hindbrain boundary, eye, branchial arches, and otic vesicle in wild-types and heterozygotes, while intestinal expression had decreased compared to 3 dpf. At 5 dpf, *ezh2* expression was clearly visible in the mid-hindbrain boundary and otic vesicle in wild-types and heterozygotes. At 3, 4, and 5 dpf, *ezh2* expression was visibly decreased in heterozygotes and predominantly diminished in *ezh2*<sup>-/-</sup> embryos through nonsense-mediated decay. Overall, *ezh2* expression detected by WISH in wild-types was consistent with RT-qPCR data presented in Figure 3A. Western blot analysis of whole larvae at 5 dpf indicated that the Ezh2 protein is diminished and H3K27me3 is decreased in *ezh2*<sup>-/-</sup> larvae compared to wild-types.

## 2.7. The Digestive System in *ezh2* Mutants

After the initial characterization of the zygotic *ezh2*<sup>-/-</sup> mutant model, we looked further into the development of the embryos and larvae for phenotypes, with focus on intestinal development. We observed that around 11 dpf, a time point at which the majority of the mutants have died, *ezh2*<sup>-/-</sup> larvae appeared to be leaner (Figure 4A). Upon closer examination, we observed that both the intestinal bulb and the liver of *ezh2*<sup>-/-</sup> mutants were smaller. In addition, the liver showed signs of steatosis (lipid accumulation), indicated by its dark appearance [63].

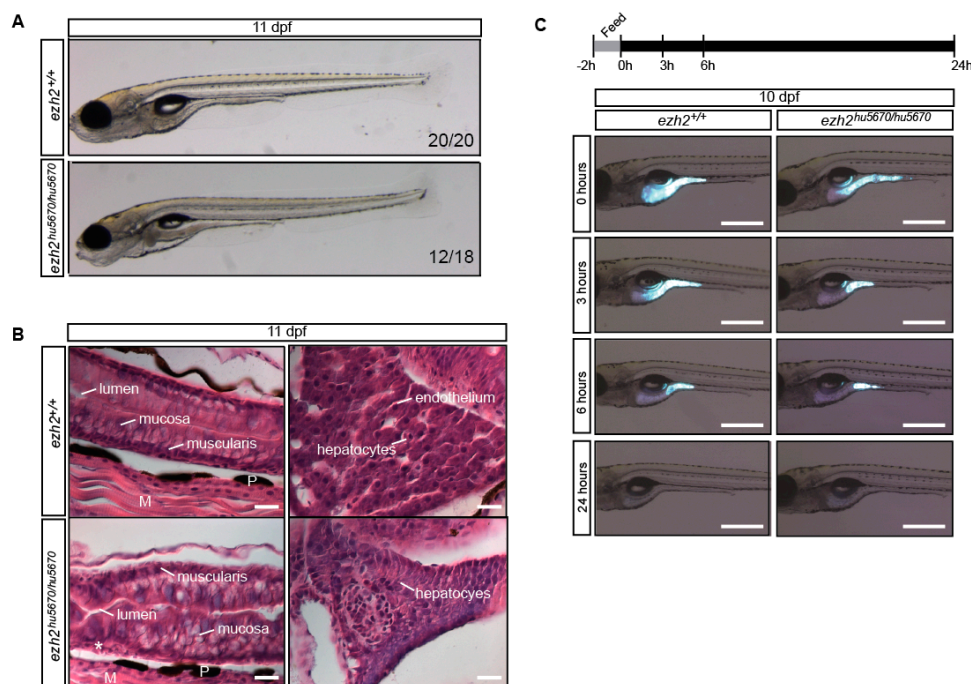
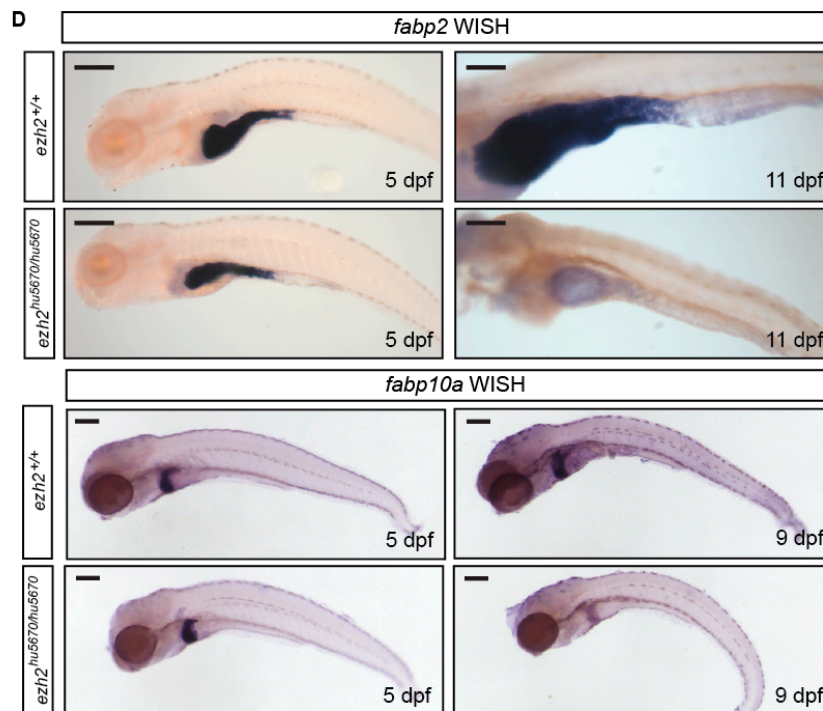


Figure 4. Cont.



**Figure 4.** The zygotic *ezh2* mutants lose intestinal and hepatic tissue maintenance yet can pass feed normally. (A) Light microscopy images of 11 dpf wild-type and *ezh2*<sup>-/-</sup> mutant larvae. The mutants seem to be smaller and leaner than wild-type siblings. Numbers indicate observation of described phenotype per total larvae analyzed; wild-types: 20/20 normal, mutants: 12/18 lean. (B) Histological analysis of wild-type siblings and *ezh2*<sup>-/-</sup> mutants at 11 dpf. The intestine and liver of wild-type siblings show a regular structure. The intestinal lumen, mucosa, and muscularis are clearly visible (top left), and the liver shows aligned hepatocytes intercepted by the endothelium (top right). The intestine of *ezh2*<sup>-/-</sup> mutants appears to be irregular in structure. The mucosa layer is disorganized and the muscularis layers appear to be partly missing (bottom left). *ezh2*<sup>-/-</sup> mutant livers are small with increased nucleocytoplasmic ratio and seem to be missing the endothelium (bottom right). Scale bar: 10  $\mu$ m; P: pigment; M: muscle; Asterisk: muscularis. (C) Intestinal transit assay in 10 dpf wild-type siblings and *ezh2*<sup>-/-</sup>. Larvae were fed with fluorescent feed for 2 h and subsequently followed for 24 h in time increments, depicted on top of the figure. The ingestion, passage, and excretion of feed in *ezh2*<sup>-/-</sup> larvae (right panel) were comparable to wild-type larvae (left panel). Scale bar: 500  $\mu$ m. (D) Whole-mount in-situ hybridization of larvae for enterocyte (*fabp2*) and hepatocyte (*fabp10a*) marker expression. At 5 dpf, heterozygous siblings and *ezh2*<sup>-/-</sup> express *fabp2* comparably in the intestinal bulb, mid-intestine, and *fabp10a* in the liver, respectively (left panels). At 11 dpf and 9 dpf, *ezh2*<sup>-/-</sup> show no *fabp2* expression and decreased *fabp10a* expression, respectively. Scale bar: 200  $\mu$ m.

Histological analysis of the mid-intestine of wildtype and *ezh2*<sup>-/-</sup> larvae at 11 dpf showed structural abnormalities. The different layers of the intestine, mucosa, and muscularis were linearly aligned along the intestinal lumen of wild-type siblings, whereas these structures appeared to be disorganized in *ezh2*<sup>-/-</sup> larvae (Figure 4B). The mucosal layer appeared thickened, and in turn, the muscularis layer was thinner in some portions of the tissue, resulting in an inconsistently shaped lumen. Transversal sections of the intestinal bulb showed no apparent disruption in intestinal fold morphology in *ezh2*<sup>-/-</sup> larvae at 10 dpf (Figure S6A). Moreover, no visible differences were detected in goblet cell numbers between the wild-type and *ezh2*<sup>-/-</sup> intestines at 5 and 10 dpf (Figure S6B).

Histological analysis of the liver also showed disorganization in the organ in *ezh2*<sup>-/-</sup> larvae at 11 dpf. In the wild-type siblings, hepatocytes were layered in sheets in an organized manner, interrupted regularly by sinus endothelium. The liver, however, was smaller in *ezh2*<sup>-/-</sup>, with a larger

nucleus-to-cytoplasm ratio than wild-types. Strikingly, the endothelium (vascular sinusoid) was not visible in the mutants.

Because we observed a disorganized lumen in *ezh2*<sup>-/-</sup> intestines, we resolved to assess intestinal transit in wild-type siblings and *ezh2*<sup>-/-</sup> at 10 dpf with the aid of fluorescent microspheres mixed with larval feed. After 2 h of fluorescent food exposure, we examined the larvae at 0, 3, 6, and 24 h post-feeding. Remarkably and rather unexpectedly, both wild-type siblings and *ezh2*<sup>-/-</sup> showed a similar intestinal transit throughout the experiment (Figure 4C).

To determine how the loss of *ezh2* affects tissue differentiation, we performed WISH for *fabp2* (at 5 and 11 dpf), an enterocyte marker, and *fabp10a* (at 5 and 9 dpf), a hepatocyte marker. Both *fabp2* and *fabp10a* were expressed in 5, 7, and 9 dpf wild-type larval intestines in our RNA-sequencing dataset (Figure 1). By WISH, no difference in gene expression patterns between wild-type siblings and *ezh2*<sup>-/-</sup> larvae was found at 5 dpf (Figure 4D). At later stages, the respective organs of wild-type fish grew, and the expression of both markers persisted. However, in *ezh2*<sup>-/-</sup> larvae, the expression of *fabp2* was visibly lost, while *fabp10a* expression was drastically reduced (Figure 4D). Taken together with the histological analysis (Figure 4B), this indicates that enterocytes and hepatocytes are formed in *ezh2*<sup>-/-</sup> larvae/embryos at 5 dpf, but the further development of intestine and liver is hampered, leading to cell loss and lethality around 11 dpf.

### 3. Discussion

Ezh2 and its functions have been studied in many model systems due to its well-recognized involvement in development and tissue maintenance. Zebrafish are an important tool in epigenetic research, yet, (epi)genetic regulation of tissue-specific development has remained a rather unexplored area. Although the whole zebrafish transcriptome has been studied at earlier stages [56], this study is noteworthy in presenting an intestine-specific analysis of the transcriptome at the early larval stages. Here, we characterized the wild-type gene expression and the presence of the H3K4me3 and H3K27me3 marks in larval zebrafish intestine and showed that the loss of Ezh2 leads to larval lethality and aberrant tissue maintenance both in the intestine and liver.

Wang and colleagues [43] previously published a microarray analysis of adult zebrafish intestines, where they divided the intestine into seven equal lengths and analyzed the gene expression. They found that gene expression patterns in the intestinal bulb, mid-intestine, and the anterior portion of posterior intestine strongly resemble those of mammalian small intestines, while most of the posterior intestine resembles the rectum of mammals. In this study, we presented a map of the zebrafish intestinal transcriptome in early larval stages, which was made possible by our novel approach of rapid and efficient intestinal dissection using the intestine-specific transgene *tgBAC(cldn15la:GFP)*.

Gene expression patterns that were commonly found across 5, 7, and 9 dpf showed that metabolic regulation is highly enriched in early larval zebrafish intestines. We were able to detect 86.5% of genes known to be expressed in zebrafish intestines in this dataset. Genes important for the lipid metabolism such as fatty acid binding proteins and apolipoprotein variants were highly expressed in the zebrafish intestine, as well as a selection of proteases. Many conserved cell signaling pathways involved in intestinal development and maintenance were also represented. Components of Wnt signaling [64], important for intestinal cell renewal, and Notch signaling [52], important for goblet cell differentiation, were expressed. GO term and anatomical term analyses confirmed that the genes in our RNA-sequencing dataset are intestinal genes, and they are enriched in the protein/peptide metabolism.

The zebrafish intestine continues maturing during the second week of development [46,65], therefore, changes in gene expression are predicted over time. A differential expression analysis between 5 and 9 dpf intestines indicated an increase in genes associated to biological processes related to cholesterol metabolism, which might reflect the transition of zebrafish from yolk-dependent embryonic stages to an independently feeding larva between 5 and 9 dpf. Before the depletion of yolk, the yolk itself can process lipids (e.g., by phospholipases) before their uptake into the embryo [66]. After 5 dpf, the embryo is reliant on a complex external lipid species as opposed to the predominant

fatty acid uptake from the yolk [67]. Therefore, it can be postulated that the lipid metabolism would be upregulated over time. Indeed, many proteasomal genes (*psm* variants), apolipoproteins, as well as acyl-coA synthases specific to long-chain fatty acids (*acsl* variants) were upregulated between 5 and 9 dpf larvae.

Genes downregulated between 5 and 9 dpf were enriched for cellular component organization or biogenesis. Amongst the downregulated genes were also transcription and growth factors involved in early development such as the *klf*, *fox*, *fos*, *bmp*, *fgf*, and *smarca* variants, as well as genes involved in chromatin dynamics such as *jmj/kdm* histone demethylase variants. In vertebrates, in general, during lineage commitment, the expression of developmental regulators changes in a tissue-specific manner, and pluripotency/growth factors get downregulated by epigenetic regulation [68]. Therefore, as the larval zebrafish intestine matures, the downregulation of developmental genes may be predicted.

In our ChIP-sequencing dataset in the intestine, we detected 5.7 times more promoters marked by H3K4me3 than H3K27me3. This is a pattern similar to early zebrafish development, where H3K4me3 marks more promoters than H3K27me3 (e.g., 5 times more in the 256-cell stage) [41]. On average, 95% of H3K4me3-marked genes, as well as a remarkable 85% of H3K27me3-marked genes were active. Interestingly, both marks were enriched on the promoters of genes involved in metabolic pathways, further emphasizing the importance of metabolic processes in the intestine. However, a comparison of gene expression levels between the two marks indicated that on average, H3K27me3 marked genes were expressed at much lower levels, depicted in Figure 2B,E. This trend might result from the fact that the whole intestinal tissue was analyzed as opposed to single cells. In a mix of different cells and tissues, cellular differences might mask the cell-specific repression/activation status of genes. Similarly, a false positive co-occupancy of the H3K4me3 and H3K27me3 marks may be observed on the same gene promoter. A gene that is repressed in most intestinal cells might be activated in others, resulting in a low number of reads during RNA-sequencing as was observed for H3K27me3-marked genes. Nevertheless, GO-term and anatomical term analyses indicate that gene promoters marked in high levels by H3K27me3 might be extra-intestinal genes; neuronal cell adhesion is apparently repressed in the zebrafish larval intestine.

Studies in the mouse intestine indicate that PRC2-mediated gene repression is crucial for correct intestinal development and survival into adulthood. The conditional knockout of the PRC2 subunit Eed in postnatal intestinal crypts results in smaller intestines with decreased stem cell pools, decreased proliferation potential, and increased secretory (goblet) cell differentiation [69]. In contrast, the conditional knockout of Ezh2 in the mouse intestine shows relatively normal proliferation in the crypts, and decreased but not diminished H3K27me3 levels [69,70]. The lack of a PRC2-null phenotype in these Ezh2 mutants, which lose Ezh2 protein expression, might be explained by the redundant function of Ezh1 [29,69,70]. Moreover, the PRC2 complex is thought to prevent the over-proliferation of goblet cells in mouse intestines through the regulation of Notch signaling [71]. All of the abovementioned epigenetic studies on the mammalian intestine, as well as studies on the liver [33], report decreased tissue size or mass upon loss of PRC2 function, which was also observed in this study.

Zebrafish zygotic *ezh2* mutants surprisingly died only at the larval stages, around 11 dpf. Considering the developmental time span, this relatively late lethality is unusual for the loss of a protein essential for early embryonic development. It is prudent to mention that the maternal *ezh2* load is present in this mutant model, which means that the loss of the Ezh2 protein expression and the H3K27me3 mark is likely delayed, which in turn may cause a delay in tissue maintenance defects. The fact that it is the intestinal tissue which shows a significant *ezh2* related phenotype might be explained by the highly proliferative nature of the vertebrate intestine compared to other tissues [72], as loss of PRC2 leads to decreased proliferation [70]. Studies in mammals point out that a complete tissue-specific PRC2 knockout phenotype cannot be generated by the loss of Ezh2 alone in differentiated tissues, due to the redundancy of its homolog Ezh1 [29,69,70]. In-vitro studies in mice and fruit flies have shown that Ezh1 is able to take over canonical and non-canonical [13]

methyltransferase functions of Ezh2, although it is catalytically less active than Ezh2 [58,59]. Indeed, the *ezh1* mRNA is expressed at 5, 7, and 9 dpf in the wild-type intestine, as shown in Figure 1A in this study. Thus, the presence of the Ezh1 protein in the zebrafish intestine might compensate for the (partial) retention of the H3K27me3 mark on the intestinal tissue in *ezh2*<sup>-/-</sup> larvae and delay the observed phenotypes, although the loss of *ezh2* is still ultimately lethal.

Our experiments using *ezh2*<sup>-/-</sup> zebrafish larvae further resulted in the confirmation of a tissue maintenance phenotype. Despite the loss of tissue maintenance in the intestine, peristalsis, which is predominantly controlled by enteric neurons and smooth muscles [47], was normal. Intestines and livers of *ezh2*<sup>-/-</sup> larvae were smaller and disorganized, and they gradually lost the expression of tissue-specific markers *fabp2* and *fabp10a*, respectively. This suggests that terminal differentiation is unaffected in *ezh2*<sup>-/-</sup> mutants, yet the differentiated tissues cannot be maintained over time. In relation to the loss of enterocyte marker expression, it can be speculated that food absorption might be affected in the intestine, contributing to the leanness of the larvae and eventually to larval lethality. However, due to our observation that intestinal fold morphology is majorly unchanged in the *ezh2*<sup>-/-</sup> intestinal bulb at 10 dpf (Figure S6A), we do not predict severe defects in food absorption in mutants.

We have previously reported the effects of the loss of maternal and zygotic *ezh2* during early zebrafish development, using the ENU-mutagenized zebrafish strain *ezh2(hu5670)*, which harbors a nonsense mutation upstream of the methyltransferase domain [60]. These maternal-zygotic *ezh2* mutants formed a normal body plan with a pleiotropic phenotype in eye, heart, liver, intestine, and pancreas before lethality at 2 dpf, indicating a role for Ezh2 in regulating tissue maintenance in the intestinal tract [60], amongst others. In another study with the zygotic *ezh2(ul2)* nonsense mutant model, the aberrant development of intestine and pancreas, and lethality around 12 dpf was reported [73], which proved the similarities with the *ezh2(hu5670)* mutant phenotypes that we present in this study.

We conclude that wild-type intestinal tissue in early zebrafish larvae expresses genes that maintain metabolic processes and signaling pathways important for intestinal development and undergoes changes in gene expression that lead to an increase in lipid metabolism in this transitional period for establishing independent feeding. During this time, H3K4me3 and H3K27me3 both mark promoters of genes, where presence of high H3K4me3 and low H3K27me3 peaks correlates with high gene expression rates. According to our study in *ezh2*<sup>-/-</sup> larvae, the H3K27me3 mark placed on the genome at early embryonic stages by maternal Ezh2 seems to suffice for successful gastrulation and tissue specification. However, at later stages, there is a gradual loss of gene regulation control in the absence of Ezh2, leading to loss of intestinal and hepatic tissue maintenance and larval lethality.

## 4. Materials and Methods

### 4.1. Zebrafish Husbandry and Strains

Zebrafish (*Danio rerio*) were housed under standard conditions in a 14:10 light/dark cycle. Embryos were reared in E3 medium at 28.5 °C [74] and staged following Kimmel et al. [75]. Larvae were fed a standard Gemma Micro 75 (Skretting USA) diet, supplemented with rotifer (*Brachionus* spp.), polyculture, and Artemia according to guidelines [76]. The *ezh2* nonsense mutant (*hu5670*, R592STOP) was derived from ENU random mutagenized libraries as described [60]. Adult zebrafish heterozygous for the *ezh2* mutant allele (*ezh2*<sup>+/-</sup>) were out-crossed against wildtype TL zebrafish for the maintenance of the line, and in-crossed to obtain homozygous mutants (*ezh2*<sup>-/-</sup>). The heterozygous in-cross generated embryos with genotypes in a Mendelian ratio. The *tgBAC (cldn15la:GFP)* zebrafish has been described before and is represented by the genomic feature *pd1034Tg* [54]. Zebrafish older than 2 dpf were anesthetized in 2-phenoxyethanol (0.05% *v/v*, Sigma Aldrich, 122-99-6) and handled immediately upon the halt of twitch response. Euthanasia was performed by immersion in 0.1% (*v/v*) 2-phenoxyethanol. All experiments were carried out in accordance with animal welfare laws, guidelines, and policies, and were approved by the Committee on the Ethics of Animal Experiments of

the VU University Amsterdam (IVM 14-01) and by the Central Committee for Animal Experimentation (CCD) of The Netherlands (AVD1030020184668, approved 26 February 2018).

#### 4.2. Intestinal Dissections

Overnight-starved wild-type zebrafish larvae of 5, 7, and 9 dpf in the *tgBAC* (*cldn15la:GFP*) background were anesthetized and their intestines were dissected under fluorescence light microscopy (Leica MZ FLIII; Leica, Wetzlar, Germany). Adhering tissues were cleaned off using watchmakers' tweezers and a microsurgical blade. Single intestines were promptly transferred to 1.5 mL microcentrifuge tubes by glass Pasteur pipettes, and lysed for RNA isolation or fixed for chromatin extraction (see below).

#### 4.3. RNA-Sequencing

Pools of 10 intestines in three biological replicates were lysed in Trizol (Thermo Fisher Scientific, 15596018; Waltham, MA, USA) and the total RNA was isolated using in-column DNase I treatment (Quick RNA microprep kit, Zymo Research, R1051, Irvine, CA, USA). Upon ribosomal RNA depletion (RiboZero Gold, Illumina MRZH11124, San Diego, CA, USA), the RNA integrity number (RIN) was assessed to be  $\geq 8$  (Agilent 2100 Bioanalyzer, G2939BA; Agilent Technologies, Santa Clara, CA, USA) with the use of an RNA 6000 Pico kit (Agilent, 5067-1513). The RNA was then fragmented to 250–300 bp and reverse-transcribed into double-stranded cDNA. Sequencing libraries were prepared with the Kapa Hyper Prep kit (KAPA Biosystems, KK8504; Wilmington, MA, USA) with NextFlex ChIP-sequencing barcodes (BioScientific, 512913; Seattle, WA, USA), and sequenced on the Illumina NextSeq500 platform (43 bp, paired-end). Reads were mapped to the *Danio rerio* genome GRCz10/danRer10 with the Ensembl gene annotation v87 using STAR [77] version 2.5.2b with default parameters and `–quantMode on “GeneCounts”`. The library quality was checked and confirmed to be sufficient for further analysis (Table S14). Differential gene expression was calculated using DeSeq2 [78] with an adjusted p-value threshold of  $< 0.01$  and a  $\log_2$  fold change of  $\neq 0$ . An FPKM  $\geq 1$  standard for 2 out of 3 replicates from all time points was set for accepting that a gene was expressed in the dataset. Cell type-specific genes used for  $\chi^2$  significance test and Figure S1 were extracted from The Zebrafish Information Network (ZFIN) gene expression database with larval stage filtering (3–30 dpf). Groups of genes were checked for GO-term enrichment by GOrilla (Gene Ontology enRiChment anaLysis and visualizAtion tool) [79], and for anatomical term enrichment by ZEOGS (Zebrafish Expression Ontology of Gene Sets), filtered by 7–13 dpf larval stage [80]. Full lists of GO terms, anatomical terms, and the list of term-associated genes of the top 5000 highest expressed, 2153 upregulated, and 349 downregulated genes have been given in Tables S1, S2, and S3, respectively. The 5 dpf whole larval transcriptome data were obtained from publicly available European Nucleotide Archive under accession number ERP014517 [61]. Intestine-specific RNA-sequencing data generated for this publication have been deposited in NCBI's Gene Expression Omnibus and are accessible through GEO Series accession number GSE64618.

#### 4.4. ChIP-Sequencing

Thirty intestines were dissected and pooled in 1.5 mL micro-centrifuge tubes coated with 5% BSA (Sigma, Saint Louis, MO, USA) in two biological replicates per ChIP. Protein-DNA cross-linking was performed in 1% paraformaldehyde (Thermo Fisher Scientific, 50-00-0; Waltham, MA, USA) in PBS. The reaction was quenched with 125 mM glycine and the samples were washed 3 times in PBS. Lysis and sonication (6 cycles of 30 s, PicoBioraptor, Diagenode) were performed in 20 mM Tris-HCl pH 7.5, 70 mM KCl, 1 mM EDTA, 10% glycerol, 0.125% NP40, protease inhibitors (1 $\times$  cOmplete EDTA free, Roche, 11873580001; Basel, Switzerland). One-sixth of the lysed sample (~5 intestines) was set aside as the ChIP input control. Chromatin fragments were mixed with an equal volume of IP buffer (50 mM Tris-HCl pH 7.5, 100 mM NaCl, 2 mM EDTA, 1% NP-40, protease inhibitors) and incubated with 2  $\mu$ g anti-H3K4me3 (Millipore 04-745, 2  $\mu$ g; Burlington, MA, USA) or anti-H3K27me3 (Millipore

07-449, 2 µg) antibodies overnight at 4 °C. The antibody-chromatin mix was bound to protein G magnetic beads (Invitrogen, 1003D; Carlsbad, CA, USA) and washed with (1) IP buffer and 0.1% Sodium deoxycholate; (2) IP buffer, 0.1% Sodium deoxycholate, and 400 mM NaCl; (3) IP buffer, 0.1% sodium deoxycholate, and 250 mM LiCl. The immunoprecipitated chromatin fragments were eluted 2 times in 50 mM NaHCO<sub>3</sub> pH 8.8, 1% SDS at 65 °C, subjected to RNase A treatment, and de-cross-linked overnight at 65 °C (200 mM NaCl, 1 mg/ml proteinase K). The eluted DNA was purified (MinElute Reaction clean-up kit, Qiagen, 28204; Hilden, Germany) and prepared for sequencing using the KAPA Hyper Prep Kit (KAPA Biosystems, KK8504) with NextFlex ChIP-sequencing barcodes (BioScientific, 514122). Sequencing was performed with the Illumina NextSeq500 platform (43 bp, paired-end). Reads were mapped to the *Danio rerio* genome GRCz10/danRer10 with the use of BWA [81] version 0.7.15 with default settings. The library quality was checked and confirmed to be sufficient for further analysis (Table S14). Multi-mappers were excluded with the use of samtools [82] version 1.3.1 and duplicate reads were removed with Picard [83]. Peaks were called by the use of MACS2 [84] version 2.1.1.20160309 relative to the ChIP input with the options -f BAMPE -g 1.3e9 -q 1e-4 -broad -broad-cutoff 1e-3. Peaks with 1 kb or a closer distance to each other were merged. Only intersecting peaks between replicates were considered with the use of GenomicRanges [85]. Peaks overlapping promoter regions (400 nt upstream–100 nt downstream of the transcriptional start site) were clustered using the union of the remaining peaks found in H3K4me3 and H3K27me3 ChIPs. Clustering and visualization of the peaks were done using fluff [86] version 2.1.3. Names of genes which were marked by H3K4me3 and/or H3K27me3 on promoters were extracted for comparison with RNA-sequencing results. Groups of genes were checked for GO-term enrichment by GOrilla (Gene Ontology enrichment anaLysis and visualiZation tool) [79], and for anatomical term enrichment by ZEOGS (Zebrafish Expression Ontology of Gene Sets), filtered by 7–13 dpf larval stage [80]. Full lists of GO terms, anatomical terms, and the list of term-associated genes of the top 5000 highest expressed H3K4me3-marked genes, H3K27me3-marked genes, genes marked by both H3K4me3 and H3K27me3, and clusters 1, 2, 3, and 4 have been given in Tables S7, S8, S9, S10, S11, S12, and S13, respectively. ChIP-sequencing data discussed in this publication have been deposited in NCBI's Gene Expression Omnibus and are accessible through GEO Series accession number GSE64618.

#### 4.5. Genotyping

For standard genotyping of live and fixed material, caudal fins of 2 or 3 dpf anesthetized embryos were clipped with a microsurgical blade. The tissue was lysed in 25 mM NaOH and 0.2 mM EDTA at 95 °C and the solution was subsequently neutralized with an equal volume of 40 mM Tris-HCl (pH predicted to be 5). To genotype single 5 dpf larvae for Western blot, 0.5 µL protein extract (see Section 4.9) was digested in a lysis buffer (50 mM KCl, 2.5 mM MgCl<sub>2</sub>, 10 mM Tris-HCl pH 8, 0.45% NP-40, 0.45% Tween-20, 0.01% gelatin, 100 µg/mL proteinase K) for 1 h at 60 °C and 15 min at 95 °C. After either method of tissue lysis, the genomic region flanking the *ezh2* (*hu5670*) mutation site (exon 14-15) was amplified by a nested PCR reaction. Primer sequences can be found in Table 1. The C>T mutation in this allele generated an additional RsaI site, which allowed for the identification of genotypes by differential restriction digestion patterns of the PCR-amplified fragments. The digests were analysed by agarose gel electrophoresis to determine the genotypes.

**Table 1.** The nested PCR primer sequences for *ezh2* exon 14-15 amplification for *ezh2* (*hu5670*) genotyping.

Primers	Primer Sequences (5' to 3')
Nested PCR 1, <i>ezh2</i> forward	CAGAATCGGTTTCCAGGTTGCCG
Nested PCR 1, <i>ezh2</i> reverse	CAGTACTCTGAGATGAACTCATTC
Nested PCR 2, <i>ezh2</i> forward	TGTAAAACGACGGCCAGTCAGAATCGGTTTCCAGGTTGCCG
Nested PCR 2, <i>ezh2</i> reverse	AGGAAACAGCTATGACCATTGCAGGAGACGTTTTTACTGTCCC

#### 4.6. Survival Assay

Embryos (3 dpf) were genotyped as described above. Wild-type ( $n = 43$ ) and mutant ( $n = 49$ ) larvae were transferred to the juvenile husbandry system at 5 dpf. Dead embryos and larvae were collected daily to assess survival.

#### 4.7. Quantitative Real-Time PCR Analysis

Wild-type embryos and larvae were staged in a time series from the 4–16 cell stage to 15 dpf and homogenized (Bertin Instruments, Precellys<sup>®</sup> 24; Montigny-le-Bretonneux, France) 2 times for 30 s at 6000 rpm. RNA extraction was performed with the use of the NucleoSpin 8 RNA kit (Machery-Nagel, 740465.4; Düren, Germany) with vacuum extraction. A total of 1 µg of RNA was used for cDNA synthesis using the high-capacity cDNA synthesis kit (Thermo Fisher Scientific, 4368814; Waltham, MA, USA). Standard qPCR was performed (SYBR Green, Bio-Rad, Hercules, CA, USA) with 4 biological and 3 technical replicates and analyzed as described [87]. Relative expression levels were calculated in comparison to an average of the reference genes  $\beta$ -actin, *hprt1*, *rps18*, and *ef1a*. Primer sequences are given in Table 2.

**Table 2.** The quantitative real-time PCR primer sequences for *ezh1*, *ezh2*, and reference genes.

Primers	Primer Sequences (5' to 3')
RT-qPCR <i>ezh1</i> , forward	AGGAAGCGTCTAGTGAGGTCT
RT-qPCR <i>ezh1</i> , reverse	ACGCGATTTGACTGGAACA
RT-qPCR <i>ezh2</i> , forward	AAATCGGAGAAGGGTCCTGT
RT-qPCR <i>ezh2</i> , reverse	TCTGTTGGAGCTGAACATGC
RT-qPCR <i>hprt1</i> , forward	CAGCGATGAGGAGCAAGGTTATG
RT-qPCR <i>hprt1</i> , reverse	GTCCATGATGAGCCCGTGAGG
RT-qPCR <i>rps18</i> , forward	CATCCCAGAGAAGTTTCAGCACATC
RT-qPCR <i>rps18</i> , reverse	CGCCTTCCAACACCCTTAATAGC
RT-qPCR <i>ef1a</i> , forward	TTGAGAAGAAAATCGGTGGTGCTG
RT-qPCR <i>ef1a</i> , reverse	GGAACGGTGTGATTGAGGGAAATTC
RT-qPCR <i>b-actin</i> , forward	CGAGCAGGAGATGGGAAC
RT-qPCR <i>b-actin</i> , reverse	CAACGGAAACGCTCATTGC

#### 4.8. Whole-Mount In-Situ Hybridization

Embryos and larvae were fixed in 4% paraformaldehyde (Sigma Aldrich, 158127) in PBS at 4 °C overnight, and whole-mount in-situ hybridization was performed as previously described [56]. After Proteinase K treatment, the head and body of larvae over 7 dpf were bisected to increase the permeability of the RNA probe. Proteinase K permeabilization was optimized according to the age of embryos or larvae (Table 3), and incubation was done at 37 °C. Proteinase K solution was refreshed every 30 min. Stained embryos and larvae were mounted on 3% methylcellulose and imaged by Leica MZ FLIII stereo light microscope.

**Table 3.** The Proteinase K incubation conditions \*.

Age	Proteinase K concentration	Incubation Time **
3 dpf	5 µg/mL	90 min
4 dpf	10 µg/mL	35 min
5 dpf	15 µg/mL	55 min
9 dpf	40 µg/mL	70 min
11 dpf	40 µg/mL	80 min

\* All Proteinase K incubations were done in a 37 °C water bath. \*\* Proteinase K solution was refreshed every 30 min.

#### 4.9. Western Blotting

Single wild-type, *ezh2*<sup>+/-</sup>, and *ezh2*<sup>-/-</sup> zebrafish larvae (5 dpf siblings) were homogenized with a pestle attached to a rotor (Sigma-Aldrich, Z359971-1EA) in 5 µl RIPA buffer per larva (100 mM Tris-HCl pH 8, 300 mM NaCl, 2% NP-40, 1% Sodium deoxycholate, 0.2% Sodium dodecyl sulfate, 20% glycerol, 1 × cOmplete EDTA-free protease inhibitor cocktail (Roche, 04693159001)), genotyped, and pooled. Protein lysates were sonicated for two cycles of 15 s (PicoBioruptor, Diagenode, Liège, Belgium) at 4 °C and subsequently cleared by centrifugation for 12 min at 16,000 g at 4 °C. A total of 20 µg protein was mixed with SDS containing sample loading buffer, denatured at 95 °C for 5 min, loaded on a 4–15% gradient protein gel (Mini-Protean TGX, Bio-Rad, 456-8084), and analyzed by Western blot. Primary antibodies used for immunoblotting were anti-Ezh2 (Cell Signaling Technology, 5246S; Danvers, MA, USA), anti-H3K27me3 (Millipore, 07-449), and anti-β-Actin (Sigma-Aldrich, A5316). HRP-conjugated anti-rabbit secondary antibody (Dako, P0217, Glostrup, Denmark) incubation was followed by protein detection with the use of ECL Select Western Blotting Detection Reagent (GE Healthcare, RPN2235; Chicago, IL; USA) on an ImageQuant LAS 4000 (GE Healthcare).

#### 4.10. Histological Analysis

Zebrafish larvae were fixed overnight in 4% paraformaldehyde (Sigma Aldrich, 158127) at 4 °C. After fixation, the embryos were gradually transferred to 75% ethanol and embedded in plastic for sectioning. Plastic sections were stained with haematoxylin and eosin for histological analysis as described [57] and imaged by light microscopy (Leica DM2500).

#### 4.11. Intestinal Transit Assay

The embryos were raised to larval stages and fed as described in Section 4.1. The experimental setup was adapted from Field et al. [88] for 10 dpf zebrafish larvae. Standard larval feed (Gemma Micro 75, Skretting, Stavanger, Norway) was mixed with microspheres (FluoSpheres<sup>®</sup> Carboxylate-Modified Microspheres, 2.0 µm, yellow-green fluorescent (exc 505 nm/em 515 nm), 2% solids; Invitrogen, Carlsbad, CA, USA) and fed to overnight-starved larvae as described [88]. For each observation at 0, 3, 6, 24 h post-feeding, live larvae were anesthetized, mounted in 3% methylcellulose for fluorescent light microscopy imaging (Leica MZ FLIII), and placed back to the system water for recovery. The larvae were genotyped upon completion of the experiment.

#### 4.12. Alcian Blue Staining

Larvae aged 5 and 11 dpf were fixed in 4% paraformaldehyde (Sigma Aldrich, 158127) in PBS at 4 °C overnight, then washed several times in distilled water. The larvae were incubated in alcian blue staining solution (70% ethanol, 50 mM MgCl<sub>2</sub>, 20% distilled water, 0.02% w/v alcian blue) for 1 h or until dark blue color is visible in cartilage tissue and goblet cells. After extensive washes in distilled water, the larvae were bleached (90% distilled water, 1% w/v KOH, 0.2% v/v Triton X-100, 500 mM H<sub>2</sub>O<sub>2</sub>) for 20 min, or until the eyes got de-pigmented. Subsequently, the larvae were washed in demi-water several times and incubated in a digestion medium (1 mg/mL Trypsin, 60% w/v borax, 0.2% v/v Triton X-100). Finally, the larvae were washed once, destained (20% glycerol and 0.25% w/v KOH in distilled water) for 30 min, and imaged (Leica MZ FLIII).

**Supplementary Materials:** The following are available online at <http://www.mdpi.com/2075-4655/2/4/19/s1>.

**Author Contributions:** Conceptualization, B.S., K.V. and L.M.K.; Data curation, B.S., M.A., D.M.E., K.V., M.d.B., J.R., and L.M.K.; Formal analysis, B.S., M.A., D.M.E., K.V., M.J.d.B., J.R., and L.M.K.; Funding acquisition, J.L., and L.M.K.; Investigation, B.S., M.A., D.M.E., K.V., M.J.d.B., J.R., and L.M.K.; Methodology, B.S., K.V., M.J.d.B., and L.M.K.; Project administration, B.S., M.A., K.V., and L.M.K.; Resources, B.S., M.A., D.M.E., K.V., M.J.d.B., J.L., and L.M.K.; Software, B.S. and D.M.E.; Supervision, B.S. and L.M.K.; Validation, B.S., M.A., K.V., M.J.d.B., J.R., J.L., and L.M.K.; Visualization, B.S., D.M.E., K.V., M.J.d.B. and L.M.K.; Writing—original draft, B.S. and L.M.K.; Writing—review & editing, B.S., M.A., D.M.E., K.V., M.J.d.B., J.R., J.L., and L.M.K.

**Funding:** This research was funded by the Innovative Research scheme of the Netherlands Organisation for Scientific research ([www.nwo.nl](http://www.nwo.nl), NWO-Veni 916.96.021, NWO-Vidi 864.12.009, and NWO-Vidi 864.09.005) and the Radboud University Nijmegen Medical Centre tenure track fellowship ([www.radboudumc.nl](http://www.radboudumc.nl)).

**Data Availability:** RNA-sequencing and ChIP-sequencing data from this manuscript have been deposited in NCBI's Gene Expression Omnibus and are accessible through GEO Series accession number GSE118076.

**Acknowledgments:** The authors thank Peter van Maurik for his work on the *ezh2(5670)* allele at the Hubrecht Institute, Tom Spanings and Antoon van der Horst of Radboud University for zebrafish husbandry, Gert Flik of Radboud University for hosting the zebrafish and for scientific discussions, René F. Ketting of Institute for Molecular Biology for scientific support and discussions, Eva Janssen-Megens of Radboud University for sequencing assistance, Sylvia Boj of Utrecht University for the *fabp2* probe, Jeroen Korving of the Hubrecht Institute for histological assistance, Ashley Alvers and Michel Bagnat of Duke University for the *tgBAC(cldn15la:GFP)* line.

**Conflicts of Interest:** The authors declare no conflict of interest.

## References

- Birnbaum, K.D.; Kussell, E. Measuring cell identity in noisy biological systems. *Nucleic Acids Res.* **2001**, *39*, 9093–9107. [[CrossRef](#)] [[PubMed](#)]
- Efroni, I.; Ip, P.-L.; Nawy, T.; Mello, A.; Birnbaum, K.D. Quantification of cell identity from single-cell gene expression profiles. *Genome Biol.* **2015**, *16*, 9. [[CrossRef](#)] [[PubMed](#)]
- Bowman, G.D.; Poirier, M.G. Post-Translational Modifications of Histones That Influence Nucleosome Dynamics. *Chem. Rev.* **2015**, *115*, 2274–2295. [[CrossRef](#)] [[PubMed](#)]
- Geisler, S.J.; Paro, R. Trithorax and Polycomb group-dependent regulation: A tale of opposing activities. *Development* **2015**, *142*, 2876–2887. [[CrossRef](#)] [[PubMed](#)]
- Dong, X.; Weng, Z. The correlation between histone modifications and gene expression. *Epigenomics* **2013**, *5*, 113–116. [[CrossRef](#)] [[PubMed](#)]
- Hosogane, M.; Funayama, R.; Shirota, M.; Nakayama, K. Lack of Transcription Triggers H3K27me3 Accumulation in the Gene Body. *Cell Rep.* **2016**, *16*, 696–706. [[CrossRef](#)] [[PubMed](#)]
- Howe, F.S.; Fischl, H.; Murray, S.C.; Mellor, J. Is H3K4me3 instructive for transcription activation? *BioEssays* **2017**, *39*, 1–12. [[CrossRef](#)] [[PubMed](#)]
- Young, M.D.; Willson, T.A.; Wakefield, M.J.; Trounson, E.; Hilton, D.J.; Blewitt, M.E.; Oshlack, A.; Majewski, I.J. ChIP-seq analysis reveals distinct H3K27me3 profiles that correlate with transcriptional activity. *Nucleic Acids Res.* **2011**, *39*, 7415–7427. [[CrossRef](#)] [[PubMed](#)]
- Akkers, R.C.; van Heeringen, S.J.; Jacobi, U.G.; Janssen-Megens, E.M.; François, K.-J.; Stunnenberg, H.G.; Veenstra, G.J.C. A hierarchy of H3K4me3 and H3K27me3 acquisition in spatial gene regulation in *Xenopus* embryos. *Dev. Cell* **2009**, *17*, 425–434. [[CrossRef](#)] [[PubMed](#)]
- Voigt, P.; Tee, W.-W.; Reinberg, D. A double take on bivalent promoters. *Genes Dev.* **2013**, *27*, 1318–1338. [[CrossRef](#)] [[PubMed](#)]
- Margueron, R.; Reinberg, D. The Polycomb Complex PRC2 and its Mark in Life. *Nature* **2011**, *469*, 343–349. [[CrossRef](#)] [[PubMed](#)]
- Liu, X.; Yang, J.; Wu, N.; Song, R.; Zhu, H. Evolution and Coevolution of PRC2 Genes in Vertebrates and Mammals. *Adv. Protein Chem. Struct. Biol.* **2015**, *101*, 125–148. [[PubMed](#)]
- Xu, J.; Shao, Z.; Li, D.; Xie, H.; Kim, W.; Huang, J.; Taylor, J.E.; Pinello, L.; Glass, K.; Jaffe, J.D.; et al. Developmental control of Polycomb subunit composition by GATA factors mediates a switch to non-canonical functions. *Mol. Cell* **2015**, *57*, 304–316. [[CrossRef](#)] [[PubMed](#)]
- Smits, A.H.; Jansen, P.W.T.C.; Poser, I.; Hyman, A.A.; Vermeulen, M. Stoichiometry of chromatin-associated protein complexes revealed by label-free quantitative mass spectrometry-based proteomics. *Nucleic Acids Res.* **2013**, *41*, e28. [[CrossRef](#)] [[PubMed](#)]
- Gil, J.; O’Loghlen, A. PRC1 complex diversity: where is it taking us? *Trend. Cell Biol.* **2014**, *24*, 632–641. [[CrossRef](#)] [[PubMed](#)]
- Le Faou, P.; Völkel, P.; Angrand, P. The zebrafish genes encoding the Polycomb repressive complex (PRC) 1. *Gene* **2011**, *475*, 10–21. [[CrossRef](#)] [[PubMed](#)]
- Turner, S.A.; Bracken, A.P. A “Complex” Issue: Deciphering the Role of Variant PRC1 in ESCs. *Cell Stem Cell* **2013**, *12*, 145–146. [[CrossRef](#)] [[PubMed](#)]

18. Morey, L.; Aloia, L.; Cozzuto, L.; Benitah, S.A.; Di Croce, L. RYBP and Cbx7 Define Specific Biological Functions of Polycomb Complexes in Mouse Embryonic Stem Cells. *Cell Rep.* **2013**, *3*, 60–69. [[CrossRef](#)] [[PubMed](#)]
19. de Napoles, M.; Mermoud, J.E.; Wakao, R.; Tang, Y.A.; Endoh, M.; Appanah, R.; Nesterova, T.B.; Silva, J.; Otte, A.P.; Vidal, M.; et al. Polycomb Group Proteins Ring1A/B Link Ubiquitylation of Histone H2A to Heritable Gene Silencing and X Inactivation. *Dev. Cell* **2004**, *7*, 663–676. [[CrossRef](#)] [[PubMed](#)]
20. Wang, H.; Wang, L.; Erdjument-Bromage, H.; Vidal, M.; Tempst, P.; Jones, R.S.; Zhang, Y. Role of histone H2A ubiquitination in Polycomb silencing. *Nature* **2004**, *431*, 873–878. [[CrossRef](#)] [[PubMed](#)]
21. Yuan, W.; Wu, T.; Fu, H.; Dai, C.; Wu, H.; Liu, N.; Li, X.; Xu, M.; Zhang, Z.; Niu, T.; et al. Dense chromatin activates Polycomb repressive complex 2 to regulate H3 lysine 27 methylation. *Science* **2012**, *337*, 919–920. [[CrossRef](#)] [[PubMed](#)]
22. Riising, E.M.; Comet, I.; Leblanc, B.; Wu, X.; Johansen, J.V.; Helin, K. Gene silencing triggers polycomb repressive complex 2 recruitment to CpG islands genome wide. *Mol. Cell.* **2014**, *55*, 347–360. [[CrossRef](#)] [[PubMed](#)]
23. Morin, R.D.; Johnson, N.A.; Severson, T.M.; Mungall, A.J.; An, J.; Goya, R.; Paul, J.E.; Boyle, M.; Woolcock, B.W.; Kuchenbauer, F.; et al. Somatic mutations altering EZH2 (Tyr641) in follicular and diffuse large B-cell lymphomas of germinal-center origin. *Nat. Genet.* **2010**, *42*, 181–185. [[CrossRef](#)] [[PubMed](#)]
24. Villanueva, M.T. Anticancer drugs: All roads lead to EZH2 inhibition. *Nat. Rev. Drug Discov.* **2017**, *16*, 239. [[CrossRef](#)] [[PubMed](#)]
25. Donohoe, M.E.; Zhang, X.; McGinnis, L.; Biggers, J.; Li, E.; Shi, Y. Targeted Disruption of Mouse Yin Yang 1 Transcription Factor Results in Peri-Implantation Lethality. *Mol. Cell. Biol.* **1999**, *19*, 7237–7244. [[CrossRef](#)] [[PubMed](#)]
26. Jones, R.S.; Gelbart, W.M. Genetic Analysis of the Enhancer of Zeste Locus and Its Role in Gene Regulation in *Drosophila Melanogaster*. *Genetics* **1990**, *126*, 185–199. [[PubMed](#)]
27. Faust, C.; Lawson, K.A.; Schork, N.J.; Thiel, B.; Magnuson, T. The Polycomb-group gene *eed* is required for normal morphogenetic movements during gastrulation in the mouse embryo. *Development* **1998**, *125*, 4495–4506. [[PubMed](#)]
28. O'Carroll, D.; Erhardt, S.; Pagani, M.; Barton, S.C.; Surani, M.A.; Jenuwein, T. The Polycomb-Group Gene *Ezh2* Is Required for Early Mouse Development. *Mol. Cell. Biol.* **2001**, *21*, 4330–4336. [[CrossRef](#)] [[PubMed](#)]
29. Bae, W.K.; Kang, K.; Yu, J.H.; Yoo, K.H.; Factor, V.M.; Kaji, K.; Matter, M.; Thorgeirsson, S.; Hennighausen, L. The methyltransferases enhancer of zeste homolog (EZH)1 and EZH2 control hepatocyte homeostasis and regeneration. *FASEB J.* **2015**, *29*, 1653–1662. [[CrossRef](#)] [[PubMed](#)]
30. Zhang, J.; Taylor, R.J.; La Torre, A.; Wilken, M.S.; Cox, K.E.; Reh, T.A.; Vetter, M.L. *Ezh2* maintains retinal progenitor proliferation, transcriptional integrity, and the timing of late differentiation. *Dev. Biol.* **2015**, *403*, 128–138. [[CrossRef](#)] [[PubMed](#)]
31. Xu, C.-R.; Li, L.-C.; Donahue, G.; Ying, L.; Zhang, Y.-W.; Gadue, P.; Zaret, K.S. Dynamics of genomic H3K27me3 domains and role of EZH2 during pancreatic endocrine specification. *EMBO J.* **2014**, *33*, 2157–2170. [[CrossRef](#)] [[PubMed](#)]
32. Michalak, E.M.; Nacerddine, K.; Pietersen, A.; Beuger, V.; Pawlitzky, I.; Cornelissen-Steijger, P.; Wientjens, E.; Tanger, E.; Seibler, J.; van Lohuizen, M.; et al. Polycomb group gene *Ezh2* regulates mammary gland morphogenesis and maintains the luminal progenitor pool. *Stem Cells* **2013**, *31*, 1910–1920. [[CrossRef](#)] [[PubMed](#)]
33. Koike, H.; Ouchi, R.; Ueno, Y.; Nakata, S.; Obana, Y.; Sekine, K.; Zheng, Y.W.; Takebe, T.; Isono, K.; Koseki, H.; et al. Polycomb Group Protein *Ezh2* Regulates Hepatic Progenitor Cell Proliferation and Differentiation in Murine Embryonic Liver. *PLoS ONE* **2014**, *9*, e104776. [[CrossRef](#)] [[PubMed](#)]
34. Herrera-Merchan, A.; Arranz, L.; Ligos, J.M.; de Molina, A.; Dominguez, O.; Gonzalez, S. Ectopic expression of the histone methyltransferase *Ezh2* in haematopoietic stem cells causes myeloproliferative disease. *Nat. Commun.* **2012**, *10*, 623. [[CrossRef](#)] [[PubMed](#)]
35. Ezhkova, E.; Pasolli, H.A.; Parker, J.S.; Stokes, N.; Su, I.; Hannon, G.; Tarakhovsky, A.; Fuchs, E. *Ezh2* Orchestrates Gene Expression for the Stepwise Differentiation of Tissue-Specific Stem Cells. *Cell* **2009**, *136*, 1122–1135. [[CrossRef](#)] [[PubMed](#)]

36. Juan, A.H.; Derfoul, A.; Feng, X.; Ryall, J.G.; Dell'Orso, S.; Pasut, A.; Zare, H.; Simone, J.M.; Rudnicki, M.A.; Sartorelli, V. Polycomb EZH2 controls self-renewal and safeguards the transcriptional identity of skeletal muscle stem cells. *Genes Dev.* **2011**, *25*, 789–794. [[CrossRef](#)] [[PubMed](#)]
37. Wurm, S.; Zhang, J.; Guinea-Viniegra, J.; García, F.; Muñoz, J.; Bakiri, L.; Ezhkova, E.; Wagner, E.F. Terminal epidermal differentiation is regulated by the interaction of Fra-2/AP-1 with Ezh2 and ERK1/2. *Genes Dev.* **2015**, *29*, 144–156. [[CrossRef](#)] [[PubMed](#)]
38. DuPage, M.; Chopra, G.; Quiros, J.; Rosenthal, W.L.; Morar, M.M.; Holohan, D.; Zhang, R.; Turka, L.; Marson, A.; Bluestone, J.A. The Chromatin-Modifying Enzyme Ezh2 Is Critical for the Maintenance of Regulatory T Cell Identity after Activation. *Immunity* **2015**, *42*, 227–238. [[CrossRef](#)] [[PubMed](#)]
39. He, A.; Ma, Q.; Cao, J.; von Gise, A.; Zhou, P.; Xie, H.; Zhang, B.; Hsing, M.; Christodoulou, D.C.; Cahan, P.; et al. Polycomb Repressive Complex 2 Regulates Normal Development of the Mouse Heart. *Circ. Res.* **2012**, *110*, 406–415. [[CrossRef](#)] [[PubMed](#)]
40. Delgado-Olguín, P.; Huang, Y.; Li, X.; Christodoulou, D.; Seidman, C.E.; Seidman, J.G.; Seidman, J.G.; Tarakhovskiy, A.; Bruneau, B.G. Epigenetic repression of cardiac progenitor gene expression by Ezh2 is required for postnatal cardiac homeostasis. *Nat. Genet.* **2012**, *44*, 343–347. [[CrossRef](#)] [[PubMed](#)]
41. Andersen, I.S.; Lindeman, L.C.; Reiner, A.H.; Østrup, O.; Aanes, H.; Aleström, P.; Collas, P. Epigenetic marking of the zebrafish developmental program. *Curr. Top. Dev. Biol.* **2013**, *104*, 85–112. [[PubMed](#)]
42. Wallace, K.N.; Pack, M. Unique and conserved aspects of gut development in zebrafish. *Dev. Biol.* **2003**, *255*, 12–29. [[CrossRef](#)]
43. Wang, Z.; Du, J.; Lam, S.H.; Mathavan, S.; Matsudaira, P.; Gong, Z. Morphological and molecular evidence for functional organization along the rostrocaudal axis of the adult zebrafish intestine. *BMC Genom.* **2010**, *11*, 392. [[CrossRef](#)] [[PubMed](#)]
44. Field, H.A.; Ober, E.A.; Roeser, T.; Stainier, D.Y. Formation of the digestive system in zebrafish. I. liver morphogenesis. *Dev. Biol.* **2003**, *253*, 279–290. [[CrossRef](#)]
45. Field, H.A.; Dong, P.D.; Beis, D.; Stainier, D.Y. Formation of the digestive system in zebrafish. II. Pancreas morphogenesis. *Dev. Biol.* **2003**, *261*, 197–208. [[CrossRef](#)]
46. Ng, A.N.; de Jong-Curtain, T.A.; Mawdsley, D.J.; White, S.J.; Shin, J.; Appel, B.; Dong, P.D.; Stainier, D.Y.; Heath, J.K. Formation of the digestive system in zebrafish: III. Intestinal epithelium morphogenesis. *Dev. Biol.* **2005**, *286*, 114–135. [[CrossRef](#)] [[PubMed](#)]
47. Holmberg, A.; Schwerte, T.; Fritsche, R.; Pelster, B.; Holmgren, S. Ontogeny of intestinal motility in correlation to neuronal development in zebrafish embryos and larvae. *J. Fish Biol.* **2003**, *63*, 318–331. [[CrossRef](#)]
48. Turgeon, N.; Blais, M.; Delabre, J.-F.; Asselin, C. The Histone H3K27 Methylation Mark Regulates Intestinal Epithelial Cell Density-Dependent Proliferation and the Inflammatory Response. *J. Cell. Biochem.* **2013**, *114*, 1203–1215. [[CrossRef](#)] [[PubMed](#)]
49. Fussbroich, B.; Wagener, N.; Macher-Goeppinger, S.; Benner, A.; Fälth, M.; Sülthmann, H.; Holzer, A.; Hoppe-Seyler, K.; Hoppe-Seyler, F. EZH2 Depletion Blocks the Proliferation of Colon Cancer Cells. *PLoS ONE* **2011**, *6*, e21651. [[CrossRef](#)] [[PubMed](#)]
50. Richmond, C.A.; Breault, D.T. Regulation of gene expression in the intestinal epithelium. *Prog. Mol. Biol. Transl. Sci.* **2010**, *96*, 207–229. [[PubMed](#)]
51. Pack, M.; Solnica-Krezel, L.; Malicki, J.; Neuhauss, S.C.; Schier, A.F.; Stemple, D.L.; Driever, W.; Fishman, M.C. Mutations affecting development of zebrafish digestive organs. *Development* **1996**, *123*, 321–328. [[PubMed](#)]
52. Crosnier, C.; Vargesson, N.; Gschmeissner, S.; Ariza-McNaughton, L.; Morrison, A.; Lewis, J. Delta-Notch signalling controls commitment to a secretory fate in the zebrafish intestine. *Development* **2005**, *132*, 1093–1104. [[CrossRef](#)] [[PubMed](#)]
53. Lickwar, C.R.; Camp, J.G.; Weiser, M.; Cocchiari, J.L.; Kingsley, D.M.; Furey, T.S.; Sheikh, S.Z.; Rawls, J.F. Genomic dissection of conserved transcriptional regulation in intestinal epithelial cells. *PLoS Biol.* **2017**, *15*, e2002054. [[CrossRef](#)] [[PubMed](#)]
54. Alvers, A.L.; Ryan, S.; Scherz, P.J.; Huisken, J.; Bagnat, M. Single continuous lumen formation in the zebrafish gut is mediated by smoothed-dependent tissue remodeling. *Development* **2014**, *141*, 1110–1119. [[CrossRef](#)] [[PubMed](#)]
55. Westerfield, M.; Doerry, E.; Kirkpatrick, A.E.; Douglas, S.A. Zebrafish informatics and the ZFIN database. *Methods Cell Biol.* **1999**, *60*, 339–355. [[PubMed](#)]

56. White, R.J.; Collins, J.E.; Sealy, I.M.; Wali, N.; Dooley, C.M.; Digby, Z.; Stemple, D.L.; Murphy, D.N.; Billis, K.; Hourlier, T.; et al. A high-resolution mRNA expression time course of embryonic development in zebrafish. *eLife* **2017**, *6*, e30860. [[CrossRef](#)] [[PubMed](#)]
57. Oksuz, O.; Narendra, V.; Lee, C.H.; Descostes, N.; LeRoy, G.; Raviram, R.; Blumenberg, L.; Karch, K.; Rocha, P.P.; Garcia, B.A.; et al. Capturing the Onset of PRC2-Mediated Repressive Domain Formation. *Mol. Cell* **2018**, *70*, 1149–1162. [[CrossRef](#)] [[PubMed](#)]
58. Son, J.; Shen, S.S.; Margueron, R.; Reinberg, D. Nucleosome-binding activities within JARID2 and EZH1 regulate the function of PRC2 on chromatin. *Genes Dev.* **2013**, *27*, 2663–2677. [[CrossRef](#)] [[PubMed](#)]
59. Margueron, R.; Li, G.; Sarma, K.; Blais, A.; Zavadil, J.; Woodcock, C.L.; Dynlacht, B.D.; Reinberg, D. Ezh1 and Ezh2 maintain repressive chromatin through different mechanisms. *Mol. Cell* **2008**, *32*, 503–518. [[CrossRef](#)] [[PubMed](#)]
60. San, B.; Chrispijn, N.D.; Wittkopp, N.; van Heeringen, S.J.; Lagendijk, A.K.; Aben, M.; Bakkens, J.; Ketting, R.F.; Kamminga, L.M. Normal formation of a vertebrate body plan and loss of tissue maintenance in the absence of ezh2. *Sci. Rep.* **2016**, *6*, 24658. [[CrossRef](#)] [[PubMed](#)]
61. Chrispijn, N.D.; Andralojc, K.M.; Castenmiller, C.; Kamminga, L.M. Gene expression profile of a selection of Polycomb Group genes during zebrafish embryonic and germ line development. *PLoS ONE* **2018**, *13*, e0200316. [[CrossRef](#)] [[PubMed](#)]
62. Wienholds, E.; van Eeden, F.; Kusters, M.; Mudde, J.; Plasterk, R.H.A.; Cuppen, E. Efficient Target-Selected Mutagenesis in Zebrafish. *Genome Res.* **2003**, *13*, 2700–2707. [[CrossRef](#)] [[PubMed](#)]
63. Kim, S.-H.; Wu, S.-Y.; Baek, J.-I.; Choi, S.Y.; Su, Y.; Flynn, C.R.; Gamse, J.T.; Ess, K.C.; Hardiman, G.; Lipschutz, J.H.; et al. A Post-Developmental Genetic Screen for Zebrafish Models of Inherited Liver Disease. *PLoS ONE* **2015**, *10*, e0125980. [[CrossRef](#)] [[PubMed](#)]
64. Jung, H.-Y.; Jun, S.; Lee, M.; Kim, H.-C.; Wang, X.; Ji, H.; McCrear, P.D.; Park, J.-I. PAF and EZH2 Induce Wnt/ $\beta$ -Catenin Signaling Hyperactivation. *Mol. Cell* **2013**, *52*, 193–205. [[CrossRef](#)] [[PubMed](#)]
65. Wallace, K.N.; Akhter, S.; Smith, E.M.; Lorent, K.; Pack, M. Intestinal growth and differentiation in zebrafish. *Mech. Dev.* **2005**, *122*, 157–173. [[CrossRef](#)] [[PubMed](#)]
66. Fraher, D.; Sanigorski, A.; Mellett, N.A.; Meikle, P.J.; Sinclair, A.J.; Gibert, Y. Zebrafish Embryonic Lipidomic Analysis Reveals that the Yolk Cell Is Metabolically Active in Processing Lipid. *Cell Rep.* **2016**, *14*, 1317–1329. [[CrossRef](#)] [[PubMed](#)]
67. Quinlivan, V.H.; Farber, S.A. Lipid Uptake, Metabolism, and Transport in the Larval Zebrafish. *Front. Endocrinol.* **2017**, *8*, 319. [[CrossRef](#)] [[PubMed](#)]
68. Mohammad, H.P.; Baylin, S.B. Linking cell signaling and the epigenetic machinery. *Nat. Biotechnol.* **2010**, *28*, 1033–1038. [[CrossRef](#)] [[PubMed](#)]
69. Koppens, M.A.; Bounova, G.; Gargiulo, G.; Tanger, E.; Janssen, H.; Cornelissen-Steijger, P.; Blom, M.; Song, J.Y.; Wessels, L.F.; van Lohuizen, M. Deletion of Polycomb Repressive Complex 2 From Mouse Intestine Causes Loss of Stem Cells. *Gastroenterology* **2016**, *151*, 684–697. [[CrossRef](#)] [[PubMed](#)]
70. Jadhav, U.; Nalapareddy, K.; Saxena, M.; O'Neill, N.K.; Pinello, L.; Yuan, G.C.; Orkin, S.H.; Shivdasani, R.A. Acquired Tissue-Specific Promoter Bivalency Is a Basis for PRC2 Necessity in Adult Cells. *Cell* **2016**, *165*, 1389–1400. [[CrossRef](#)] [[PubMed](#)]
71. Chiacchiera, F.; Rossi, A.; Jammula, S.; Zanutti, M.; Pasini, D. PRC2 preserves intestinal progenitors and restricts secretory lineage commitment. *EMBO J.* **2016**, *35*, 2301–2314. [[CrossRef](#)] [[PubMed](#)]
72. Crosnier, C.; Stamatakis, D.; Lewis, J. Organizing cell renewal in the intestine: stem cells, signals and combinatorial control. *Nat. Rev. Genet.* **2006**, *7*, 349–359. [[CrossRef](#)] [[PubMed](#)]
73. Dupret, B.; Völkel, P.; Vennin, C.; Toillon, R.A.; Le Bourhis, X.; Angrand, P.O. The histone lysine methyltransferase Ezh2 is required for maintenance of the intestine integrity and for caudal fin regeneration in zebrafish. *Biochim. Biophys. Acta* **2017**, *1860*, 1079–1093. [[CrossRef](#)] [[PubMed](#)]
74. Westerfield, M. *The Zebrafish Book, A Guide for the Laboratory Use of Zebrafish (Danio rerio)*, 5th ed.; University of Oregon Press: Eugene, OR, USA, 2007.
75. Kimmel, C.B.; Ballard, W.W.; Kimmel, S.R.; Ullmann, B.; Schilling, T.F. Stages of embryonic development of the zebrafish. *Dev. Dyn.* **1995**, *203*, 253–310. [[CrossRef](#)] [[PubMed](#)]
76. Wilson, C. Aspects of larval rearing. *ILAR J.* **2012**, *53*, 169–178. [[CrossRef](#)] [[PubMed](#)]
77. Dobin, A.; Davis, C.A.; Schlesinger, F.; Drenkow, J.; Zaleski, C.; Jha, S.; Batut, P.; Chaisson, M.; Gingeras, T.R. STAR: ultrafast universal RNA-seq aligner. *Bioinformatics* **2013**, *29*, 15–21. [[CrossRef](#)] [[PubMed](#)]

78. Love, M.I.; Huber, W.; Anders, S. Moderated estimation of fold change and dispersion for RNA-seq data with DESeq2. *Genome Biol.* **2014**, *15*, 550. [[CrossRef](#)] [[PubMed](#)]
79. Eden, E.; Navon, R.; Steinfeld, I.; Lipson, D.; Yakhini, Z. GOrilla: A Tool For Discovery And Visualization of Enriched GO Terms in Ranked Gene Lists. *BMC Bioinf.* **2009**, *10*, 48. [[CrossRef](#)] [[PubMed](#)]
80. Prykhozhij, S.V.; Marsico, A.; Meijsing, S.H. Zebrafish Expression Ontology of Gene Sets (ZEOGS): A Tool to Analyze Enrichment of Zebrafish Anatomical Terms in Large Gene Sets. *Zebrafish* **2013**, *10*, 303–315. [[CrossRef](#)] [[PubMed](#)]
81. Li, H.; Durbin, R. Fast and accurate short read alignment with Burrows–Wheeler transform. *Bioinformatics* **2009**, *25*, 1754–1760. [[CrossRef](#)] [[PubMed](#)]
82. Li, H.; Handsaker, B.; Wysoker, A.; Fennell, T.; Ruan, J.; Homer, N.; Marth, G.; Abecasis, G.; Durbin, R.; 1000 Genome Project Data Processing Subgroup. The Sequence Alignment/Map format and SAMtools. *Bioinformatics* **2009**, *25*, 2078–2079. [[CrossRef](#)] [[PubMed](#)]
83. Broad Institute, Picard Toolkit. Available online: <http://broadinstitute.github.io/picard/> (accessed on 19 August 2018).
84. Zhang, Y.; Liu, T.; Meyer, C.A.; Eeckhoute, J.; Johnson, D.S.; Bernstein, B.E.; Nusbaum, C.; Myers, R.M.; Brown, M.; Li, W.; et al. Model-based Analysis of ChIP-Seq (MACS). *Genome Biol.* **2008**, *9*, R137. [[CrossRef](#)] [[PubMed](#)]
85. Lawrence, M.; Huber, W.; Pagès, H.; Aboyoun, P.; Carlson, M.; Gentleman, R.; Morgan, M.T.; Carey, V.J. Software for Computing and Annotating Genomic Ranges. *PLoS Comput. Biol.* **2013**, *9*, e1003118. [[CrossRef](#)] [[PubMed](#)]
86. Giorgianni, G.; van Heeringen, S.J. fluff: exploratory analysis and visualization of high-throughput sequencing data. *PeerJ* **2016**, *4*, e2209. [[CrossRef](#)] [[PubMed](#)]
87. den Broeder, M.J.; Moester, M.J.B.; Kamstra, J.H.; Cenijn, P.H.; Davidoiu, V.; Kamminga, L.M.; Ariese, F.; de Boer, J.F.; Legler, J. Altered Adipogenesis in Zebrafish Larvae Following High Fat Diet and Chemical Exposure Is Visualised by Stimulated Raman Scattering Microscopy. *Int. J. Mol. Sci.* **2017**, *18*, 894. [[CrossRef](#)] [[PubMed](#)]
88. Field, H.A.; Kelley, K.A.; Martell, L.; Goldstein, A.M.; Serluca, F.C. Analysis of gastrointestinal physiology using a novel intestinal transit assay in zebrafish. *Neurogastroenterol. Motil.* **2009**, *21*, 304–312. [[CrossRef](#)] [[PubMed](#)]



© 2018 by the authors. Licensee MDPI, Basel, Switzerland. This article is an open access article distributed under the terms and conditions of the Creative Commons Attribution (CC BY) license (<http://creativecommons.org/licenses/by/4.0/>).